Application of tin oxide-based materials in catalysis

18

Pandian Manjunathan, Ganapati V. Shanbhag
Materials Science and Catalysis Division, Poornaprajna Institute of Scientific Research (PPISR), Bengaluru, India

Chapter outline

18.1 Introduction

18.1.1 Catalysis

Catalyst is a substance which accelerates the rate of a chemical reaction without itself being consumed, and the phenomenon is known as catalysis. Catalyst offers an alternative, energetically favorable pathway for a reaction and allows selective routes to produce less or no side products [1, 2].

Catalysts are not only at the heart of making most chemicals and materials (polymers), but also play a vital role in many chemical processes such as food, pharmaceuticals, fertilizers, automobiles, and petrochemical industries [3]. Almost 90% of industrial chemical manufacturing processes heavily rely on catalysts. Among them, 80% are heterogeneous, 17% are homogeneous, and 3% are biocatalysts and, also catalysis contributes to approximately 35% of the world's gross domestic product (GDP) [4–7]. Global demand on catalysts is expected to reach 24.1 billion USD by 2018 and witnessed to grow further in the coming years [8]. Furthermore, catalysis is viewed as

Tin Oxide Materials: Synthesis, Properties, and Applications. https://doi.org/10.1016/B978-0-12-815924-8.00018-9

a key enabling technology and identified as one of the 12 principles of green chemistry [9, 10]. Nowadays, due to the modern technological advancement in analytical and characterization techniques, significant efforts have been devoted for design and development of catalysts by understanding physico-chemical properties and correlation with catalysis scientifically [11–14].

Depending on the physical phase of catalyst in the reaction medium, the catalysts are broadly classified into two major groups namely homogeneous and heterogeneous. If the catalyst and reactants are in the same phase, then it is said to be homogeneous catalysis and if they are in different phases then it is called as heterogeneous catalysis [15]. Homogeneous catalyst, in general, is more active with faster reaction rates, but it suffers from recovery of catalyst from the reaction mixture and sometimes not possible to recover completely. The use of heterogeneous catalysis offers promising advantages such as reduction in the use of auxiliary resources, reduction in waste generation during product isolation, ease of catalyst recovery, easier catalyst regeneration, and reuse methods. Therefore, it allows the process by compliance with the principles of green chemistry involving minimum environmental pollution [16, 17]. Hence, this motivated the researchers to develop the heterogeneous catalysts for various organic reactions, which is both attractive and challenging.

This chapter focuses on the types of tin oxide-based materials viz., mesoporous tin oxides, mixed and composite metal oxide, anion and cation-modified tin oxide (CaO/SnO_2, WO_3/SnO_2, and heteropoly acid supported on SnO_2), and their applications in thermocatalysis. In particular, SnO_2-Ta_2O_5, Sn^{2+}/SnO_2, and Sn_3O_4 are discussed in detail for photocatalytic applications. Furthermore, SnO_2@MoS_2 film and photosystem II (PSII) integrated in a mesoporous indium-tin oxide (mesoITO) electrode have also been elaborated for photoelectrocatalytic (PEC) reactions.

18.1.2 Tin oxide

Metal oxide is found to be an exciting material in diverse applications due to its wide variety of electronic and chemical properties. Many metal oxide materials have two unique structural features; mixed cation valences and an adjustable oxygen deficiency which are the basis for creating and tuning many chemical and physical properties. It spans a wide range of electrical properties from wide band gap insulators to metallic and superconducting. In chemical applications, metal oxides are used as catalyst supports for dispersed metal catalysis but also often exhibit catalytical activity in pure form.

Tin oxide has attracted a great interest in scientific community as tin possesses a dual valency, with tin preferably attaining an oxidation state of 2+ or 4+ [18, 19]. This dual valency facilitates a variation of the surface oxygen composition resulting in different structure-function properties [20]. The oxide form of tin exists in two types, namely stannic oxide (tin dioxide, SnO_2) and stannous oxide (SnO). Stannic oxide possesses a rutile structure, whereas stannous oxide has a less common litharge structure. SnO_2 is the most abundant form of tin oxide and is one of the technological significances in various applications [21]. SnO_2 exhibits two different crystalline phases, either a tetragonal (rutile, stable one) or an orthorhombic structure (stable at relatively high pressure) [18, 22].

Tin oxide was mainly studied as an n-type semiconductor material with a wide band gap of 3.6 eV. The SnO_2 with a rutile structure was widely applied in catalysis, gas sensors, rechargeable Li-ion batteries, transparent conducting electrodes, dye-based solar cell antistatic coatings, and other optical electronic devices [19, 23–27]. In particular, tin dioxide was studied as catalyst and support for the catalyst in several organic reactions [28–36]. The acidity of a metal oxide mainly depends on the percentage ionic character of the metal-oxygen bond and the oxidation state of the metal. A metal oxide with a low percentage ionic character and high oxidation state possesses more acidity. Among different metal oxides, SnO_2 with a lower percentage ionic character (42.2) and a higher oxidation state of 4+ (for Sn) showed high acidity which can catalyze certain reactions [31]. Owing to its interesting properties like acid-base and redox, SnO_2 is found to be an active and versatile catalytic material [32].

The structure-function properties in tin dioxide can be modulated by adopting different synthetic approaches (in-situ methods) and activation steps. In in-situ method, the properties of tin dioxide can be tuned by employing structure-directing agent (SDA) to synthesize mesoporous and/or nanosized materials. Coprecipitation method helps to prepare mixed metal oxide and composite oxides. Basically, the nature of active sites in acid catalysts (metal oxide) varies based on the coordination of metal-oxygen bond. The coordinatively unsaturated cationic sites act as Lewis acidic sites, where M^+ exposed to interact with guest molecules as an electron pair acceptor. The Brønsted acid sites originate from highly polarized hydroxyl groups, acting as proton donors [37, 38]. Furthermore, the nature of acidic properties can be tuned by activation temperature.

The generation of new and strong acidic sites in tin dioxide can be obtained by ex-situ synthetic approaches, also called as postsynthetic modification. This approach involves the impregnation of cation/anion species on tin dioxide to form supported tin oxide catalysts.

18.2 Mesoporous tin oxide

After the discovery of M41S family of materials, mesoporous materials have received a great attention due to their interesting properties like high surface area, tunable pore size, and their diverse frameworks. Pore size diameter ranging between 2 and 50 nm is said to be mesoporous material. The presence of mesopores in catalysts can overcome diffusion constraints which are observed in microporous catalysts (pore size <2 nm), and the presence of large surface area facilitates easy accessibility of active sites to the reactant molecules leading to a better catalytic performance. In addition to their wide range of applications in the field of catalysis, mesoporous materials have also been used in adsorption, sensors, lithium-ion batteries, drug delivery, and nanodevices [39–45].

Initially, siliceous mesostructured materials namely MCM-41, MCM-48, SBA-15, and KIT-6 have been synthesized via a supramolecular templating approach and were further extended to synthesize transition and main group metal oxides [46, 47]. Nonsiliceous mesoporous oxides of W, Sb, and Pb were first reported and subsequently other mesostructured oxides of Al, Ti, Nb, and Zr were synthesized by

different templating routes [48–52]. However, these nonsiliceous mesoporous metal oxide materials suffered from disadvantages such as semicrystalline pore walls, low crystallinity, and thermal stability. Nevertheless, these materials have been used in several noteworthy applications and have exhibited excellent performances.

Tin dioxide materials possessing mesoporosity can be excellent catalysts since they endow the properties of mesoporous materials and metal oxides. Mesoporous tin oxide can be synthesized by two approaches, namely, soft template (in-situ) and hard template (ex-situ) routes. In soft template route, SDAs are employed to construct the porous structure, and the commonly used SDAs are Pluronic P123, cetyltrimethylammonium bromide, and Pluronic F127 [53–60]. In hard template method, tin dioxide with self-replicate of mesoporous materials as hard templates such as MCM-41, SBA-15, KIT-16, CMK-3, and CMK-8 were also synthesized using mesoporous materials as template [52, 61–64]. The hard template route may result in more ordered mesoporous structure compared to soft template route. However, the soft template approach is found to be easier process to synthesize mesoporous materials as it involves simple steps compared to hard template route.

Metal oxides are found to be interesting materials owing to their acid-base and redox properties. The surface of metal oxides may terminate with M-OH, M-O-M, M=O, or M–(O-vacant) functionalities [65]. In addition, metal oxides containing mesoporosity can be excellent catalysts as they possess multifunctional properties like porosity, acidity, basicity, and metal function due to a combination of characteristics of mesoporous materials and metal oxides. The nature of active sites in these metal oxides can be modulated by adopting different synthetic strategies and activation steps (calcination temperature). This leads to generation of active sites with a combination of Brønsted and Lewis acidic characters [32].

Shanbhag and co-workers have studied the bare mesoporous tin dioxide as a catalyst for various organic transformations such as Prins condensation of β-pinene, oxidation of cyclohexene, and glycerol transformations such as acetylation, acetalization, carbonylation, and ketalization [31, 32]. The nature and number of acidic sites in mesoporous tin dioxide was modulated by adopting different synthetic approaches and activation steps (calcination temperature). Thus, it resulted in the generation of acidic sites with a combination of Brønsted and Lewis characters along with the variation in its structure-activity correlation. The authors understood the catalytic properties by various characterization techniques and claimed that the superior activity of mesoporous tin oxide was due to higher B/L acid ratio (Brønsted-to-Lewis), surface area, and acid strength.

In this chapter, we discuss the catalytic behavior of mesoporous tin dioxide for Prins condensation reaction of β-pinene with paraformaldehyde and ketalization of glycerol with acetone to produce nopol and solketal, respectively. The mesoporous tin oxide was prepared by template-assisted method followed by calcination at different temperatures ranging from 300°C to 500°C. The change in calcination temperature resulted in the generation of different nature of acidic sites in variable quantities which was determined by pyridine-Fourier transform infrared (FTIR) and temperature-programmed desorption of ammonia (NH_3-TPD) techniques and depicted in Table 18.1. The pyridine-FTIR study of meso-SnO_2-T showed the presence

Table 18.1 Structural and acidic properties of tin oxide catalysts [32]

Catalyst	Surface area (m^2/g)[a]	Pore volume (cc/g)[b]	Pore size (nm)[c]	Acidity measurement		
				Py-FTIR (B/L)	NH_3-TPD (mmol NH_3/g)	^1H (ppm)[d]
Meso-SnO_2-T-300	160	0.12	3.45	3.5	0.41	6.43
Meso-SnO_2-T-350	105	0.11	3.72	3.2	0.44	6.63
Meso-SnO_2-T-400	55	0.10	5.39	2.5	0.29	6.51
Meso-SnO_2-T-500	51	0.10	6.79	1.4	0.24	6.54
Meso-SnO_2-TF-350	50	0.06	5.30	3.0	0.30	6.63
Meso-SnO_2-TF-500	35	0.06	3.73	–	0.11	–
Nano-SnO_2–500	43	0.08	6.76	–	0.24	–

T = template-assisted synthesis, TF = template free synthesis.
[a] BET surface area.
[b] Total pore volume.
[c] Pore diameter.
[d] ^1H MAS NMR Chemical shift.

of both Brønsted and Lewis acidic sites with a systematic decline in B/L acid ratio (Brønsted-to-Lewis) with increase in the calcination temperature due to dehydroxylation at higher temperatures. The Brønsted acidity in the catalyst was attributed to the presence of surface Sn-OH or hydrogen-bonded Sn-OH groups, whereas Lewis acidity arises due to the framework Sn^{4+} sites [32].

The NH_3-TPD measurement of meso-SnO_2-T catalyst showed a decrease in total number of acidity with an increase in calcination temperature >350°C, which was attributed to the decrease of surface area and dehydroxylation of surface active sites at higher temperatures. Among the SnO_2 catalysts, meso-SnO_2-T-350 showed higher amount of total acidity. Interestingly, template-free tin oxide (meso-SnO_2-TF-350) showed a lower acidity than template-assisted meso-SnO_2-T-350 due to its lower surface area.

Low angle X-ray diffraction (XRD) patterns of the mesostructured tin oxide catalyst after calcination at different temperatures is shown in Fig. 18.1A. The mesoporous tin oxide calcined at 300°C showed the presence of the (100) diffraction peak at low angle due to the two-dimensional (2D) hexagonal structure. However, mesoporous tin oxide calcined ≥350°C did not show any low angle diffraction peak indicating the absence of long-range order in mesopores at higher temperatures. The wide-angle XRD patterns of calcined tin oxide catalysts show diffraction peaks assigned to a tetragonal rutile crystal structure (Fig. 18.1B).

The nitrogen sorption measurement of meso-SnO_2-T-300 and meso-SnO_2-T-350 showed H2-type hysteresis loop, indicative of cavitation effect in ink-bottle-type pores attributed to the formation of spherical pores along with the cylindrical pores present in the materials (shown in Fig. 18.1C). However, meso-SnO_2-T-400 and meso-SnO_2-T-500 possess H1-type hysteresis suggesting a well-defined cylindrical-like pore channels present in the porous system. This confirms that the calcination temperature as a predominant role in the formation of porous structure.

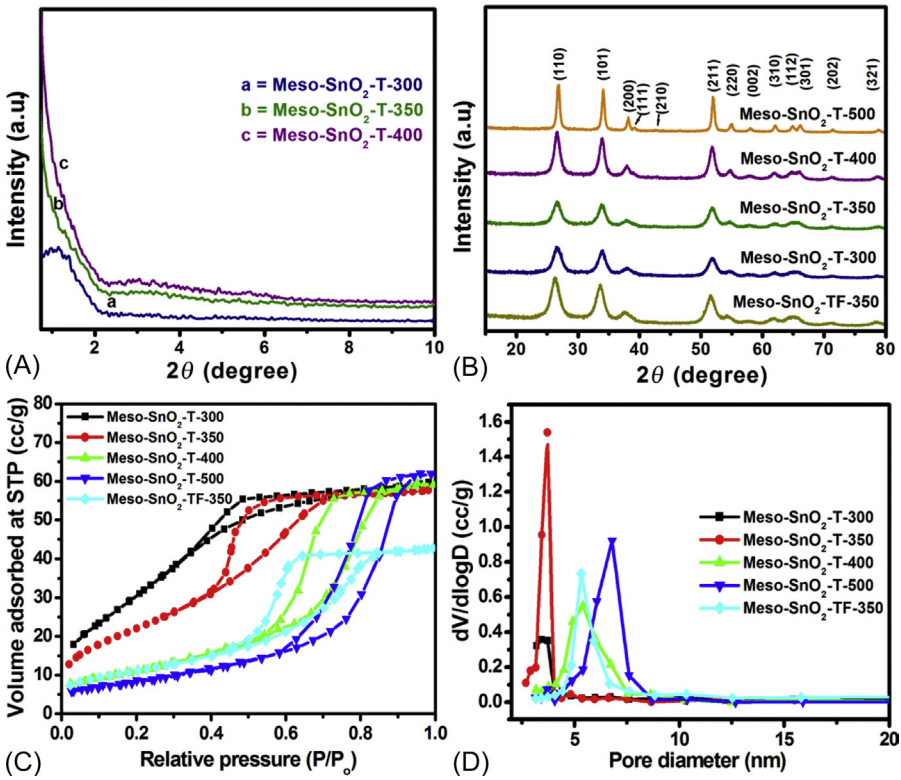

Fig. 18.1 XRD patterns at low (A) and wide (B) angle for meso-SnO_2-T-x; (C) nitrogen adsorption-desorption isotherm; and (D) pore size distribution of meso-SnO_2-T-*x*. Reprinted with permission from Manjunathan P, Marakatti VS, Chandra P, Kulal AB, Umbarkar SB, Ravishankar R, Shanbhag GV. Catal Today 2018;309:61–76. Copyright (2018) Elsevier.

The meso-SnO_2-T-300 exhibited a highest surface area of 160 m^2/g among the tin oxide catalysts. Further increase of calcination temperature >300°C resulted in significant decrease of surface area from 160 to 51 m^2/g [32].

These catalysts were evaluated for the synthesis of nopol (Scheme 18.1) by reacting activated formaldehyde with β-pinene which is one of the industrially important chemicals used in the perfumery, agrochemical, and soap-detergent industries. The electrophilic addition of aldehyde to olefin over acidic catalysts is known as the Prins reaction. This reaction requires either weak Brønsted or strong Lewis acid sites for the selective synthesis of nopol [66–69]. In this study, the authors compared the catalytic behavior of mesoporous tin oxide with tin oxide nanoparticle (nano-SnO_2-T) and template-free tin oxide (meso-SnO_2-TF). The nano and bulk tin oxide catalysts showed a lower β-pinene conversion (<25%) and a nopol selectivity of ~50% compared to the mesoporous tin oxide as shown in Fig. 18.2. The meso-SnO_2-T-350 showed a high β-pinene conversion of 80% with a nopol selectivity of 93%. Basically, β-pinene

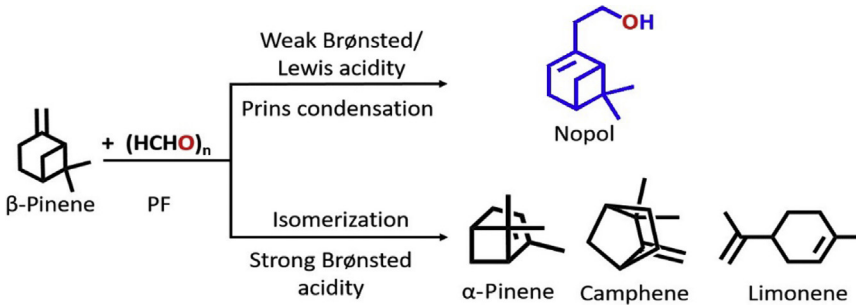

Scheme 18.1 Prins condensation of β-pinene with paraformaldehyde.

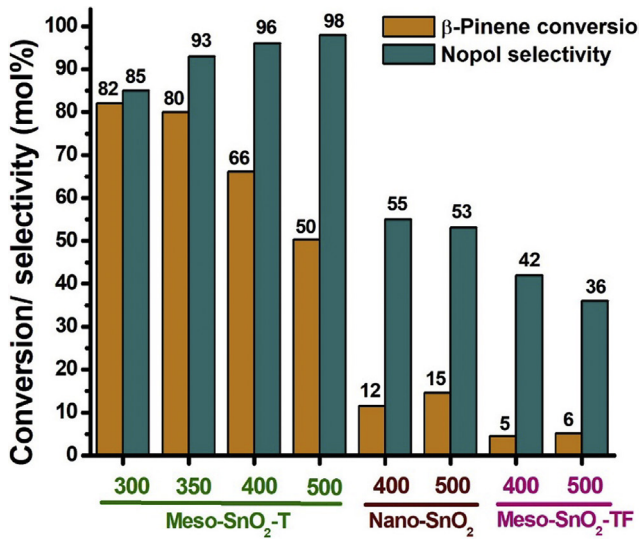

Fig. 18.2 Reaction conditions: β-pinene = 1.36 g, paraformaldehyde = 0.6 g, benzonitrile = 5 mL, catalyst amount = 0.78 g, reaction temperature = 90 °C, and reaction time = 10 h.

commonly undergoes isomerization over strong Brønsted acid catalysts to produce α-pinene, camphene, and limonene. The high selectivity for nopol (>85%) over mesoporous tin oxide catalyst was obtained due to the presence of weak acid sites on tin oxide catalyst. As the calcination temperature of mesoporous tin oxide increased from 300°C to 500°C, the conversion of β-pinene decreased from 82% to 50.4%, whereas nopol selectivity increased from 85% to 98%. The decrease of β-pinene conversion was due to the decrease of active surface acidic sites in tin oxide upon calcination. The increase of nopol selectivity was attributed to the decrease in Brønsted acid sites, because these sites are mainly responsible for the isomerization of β-pinene to side products. This reaction proves that the greater activity of mesoporous tin oxide was due to the presence of a combination of Brønsted and Lewis acidic centers.

However, the acidic strength in these catalysts was not clear from NH_3-TPD measurements since the catalysts possess low thermal stability referred to their lower calcination temperature. TPD technique depends on desorption of NH_3 molecules with respect to increase in calcination temperature. The TPD measurements beyond the calcination temperature of a metal oxide may result in the formation of H_2O molecules due to dehydroxylation which might be confused for NH_3. Further, the authors understood the acid strength in the catalyst by employing ^1H magic angle spinning nuclear magnetic resonance (MAS NMR) technique. It is an important technique which provides information about the relative strength of acidic sites in the material from the change in chemical shift due to bond polarization. Higher the chemical shift toward low field, greater is the strength of acidic sites due to a greater extent of bond polarization.

The chemical shift of template-assisted meso-SnO_2 showed an increment from 6.43 to 6.63 ppm with increase of calcination temperature from 300°C to 350°C as shown in Fig. 18.3. Interestingly, the material showed a decrease of acidic strength upon increasing of calcination temperature above 350°C with the chemical shift toward high-field from 6.63 to 6.51 ppm. Importantly, both template-free and template-assisted meso-SnO_2 calcined at 350°C showed identical chemical shift of 6.63 ppm which indicates the presence of similar strength of acidic sites in them.

Further, these catalysts were employed for ketalization of glycerol with acetone to produce solketal (5-membered) and 6-membered compounds (Scheme 18.2). Solketal can be used as a cold flow improver to enhance cold weather performance of diesel fuel and also reduces its viscosity. Solketal blended with regular gasoline in 1, 3, or 5 vol% decreases the gum formation and also it enhances the octane number up to 2.5 points [70–73]. It is also used in chemical industry as an additive in ointments for cosmetics and in low-temperature transfer fluids [74].

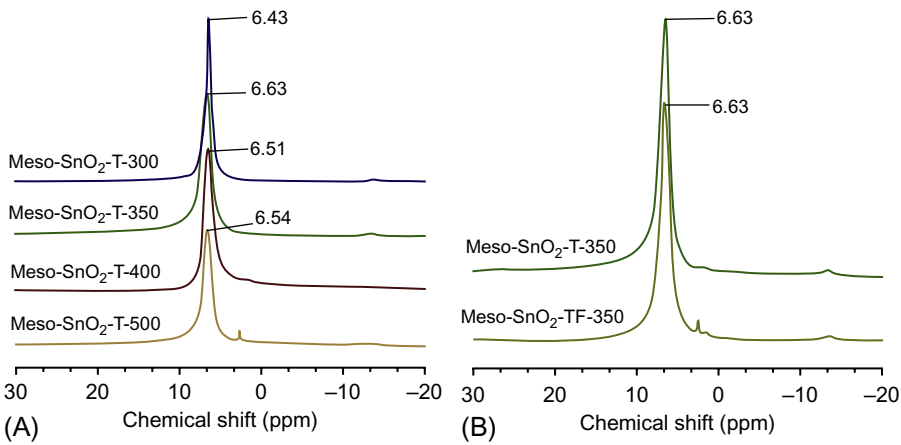

Fig. 18.3 ^1H MAS NMR (A and B) of meso-SnO_2 catalysts.
Reprinted with permission from Manjunathan P, Marakatti VS, Chandra P, Kulal AB, Umbarkar SB, Ravishankar R, Shanbhag GV. Catal Today 2018;309:61–76. Copyright (2018) Elsevier.

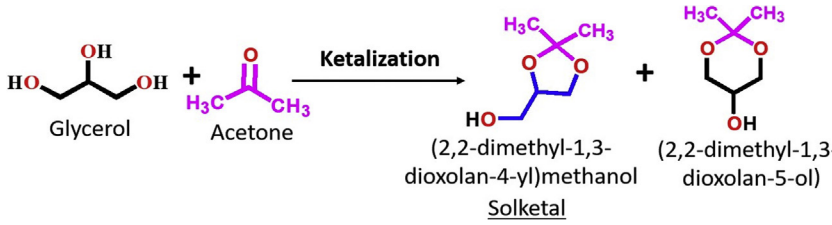

Scheme 18.2 Ketalization of glycerol with acetone

The meso-SnO_2-T-350 showed higher glycerol conversion of 51.3% with 98.0% solketal selectivity compared to other catalysts evaluated in this study and the results are shown in Table 18.2. The greater catalytic activity of meso-SnO_2-T-350 was ascribed to the presence of mesoporosity and high B/L ratio of 3.2 since this reaction is predominantly catalyzed by Brønsted acidic sites. A blank run without a catalyst showed a negligible glycerol conversion (0.1%) signifying that the reaction is truly catalytic. Importantly, the meso-SnO_2-TF-350 (template-free) catalyst showed significantly lower glycerol conversion than meso-SnO_2-T-350 (template assisted) owing to the availability of lower number of acidity and larger surface area. H-Beta zeolite with identical number of acidic sites as in meso-SnO_2-T-350 showed 38.8% glycerol

Table 18.2 Catalytic activities of different catalysts for ketalization of glycerol with acetone reaction[a] [32]

Catalyst	B/L	Acidity (mmol NH_3 des/g)	Glycerol conv. (mol%)	Solketal (mol%)		TOF (h^{-1})
				Selectivity	Yield	
Blank	–	–	0.1	90.0	0.1	–
Meso-SnO_2-T-350	3.2	0.44	51.3	98.0	50.3	506
Meso-SnO_2-TF-350	3.0	0.30	29.0	96.0	27.8	420
Al-MCM-41	1.7	1.00	35.5	94.2	33.4	154
Al-SBA-15	0.8	0.80	26.1	96.3	25.1	142
Al-TUD-1	1.9	0.98	10.2	89.0	9.1	45
H-ZSM-5	2.3	1.31	34.1	94.0	32.1	113
H-Mordenite	1.4	1.84	10.2	89.5	9.1	24
H-Beta	1.4	1.51	47.4	98.5	46.7	136
H-Beta[b]	1.4	1.51	38.8	97.6	37.9	383
Effect of calcination temperature						
Meso-SnO_2-T-300	3.5	0.41	47.6	97.5	46.4	–
Meso-SnO_2-T-350	3.2	0.44	51.3	98.5	50.5	–
Meso-SnO_2-T-400	2.5	0.29	48.7	98.5	48.0	–
Meso-SnO_2-T-500	1.4	0.24	42.4	98.5	41.8	–

T = template-assisted synthesis; *TF* = template free synthesis; *TOF (Turn over frequency)* = moles of glycerol converted per mole of acidic sites per hour.

[a] **Reaction conditions:** glycerol (27 mmol = 2.5 g), acetone (27 mmol = 1.6 g), catalyst amount = 0.125 g, temp = 60°C, time = 30 min.

[b] 0.055 mmol of acidic sites was taken.

conversion with 97.6% selectivity to solketal. Also, the authors compared the catalytic activity with other conventional micro and mesoporous acid catalysts namely H-ZSM-5, H-mordenite, H-beta, Al-MCM-41, Al-SBA-15, and Al-TUD-1. The mesoporous tin oxide outperformed other catalysts due to the presence of higher B/L acid ratio compared with other catalysts. Further, the calcination behavior of mesoporous tin oxide was studied at different temperatures ranging from 300°C to 500°C, which showed difference in catalytic activity due to the change in number of acidity. The superior catalytic behavior of meso-SnO_2-T-350 was due to the presence of higher amount of acidity than other meso-SnO_2 catalysts calcined at various temperatures.

18.3 Mixed/composite metal oxide

Mixed and composite metal oxides are widely used in industry as well as in academia which constitute one of the largest families of heterogeneous catalysts for the selective organic transformation reactions. These oxides are oxygen-containing compounds formed by the combination of two or more metal cations that may either vary or be defined by a strict stoichiometry. The original idea of preparing mixed metal oxide catalysts was to enhance the structure-function properties namely acidic or basic strength, increase the surface area, and strengthen the stability of these catalysts in comparison with single metal oxides.

Mixed metal oxides and composite metal oxides which possess different properties are differentiated by their crystalline phases. If the material exhibits a phase corresponding to individual bimetallic oxide (M_A–O–M_B), it is considered as mixed metal oxide and if it exhibits bimetallic oxide phase in addition to corresponding individual metal oxide phases, then it is said to be composite metal oxide. These oxides can be binary, ternary, quaternary, and so on depending on the number of different metal cations. These materials offer different properties compared to individual metal oxides due to the interaction of different types of metal ions connected through oxygen. The metal ions in multimetallic oxides differ in their coordination environment that governs the type of bonding between the cations resulting in synergistic effect. For example, the two different metal cations can be represented as M_A^{n+} and M_B^{m+} in polyhedra, which connect in various possible ways such as edge- or corner-sharing M_A–O–M_B–O, M_A–O–M_A–O, or M_B–O–M_B–O metal-oxygen chains. This gives different cation environments leading to different active centers and reactivity toward approaching molecule [37, 65]. More importantly, the nature of active sites in these materials can be tailored by adopting different synthetic strategies and activation steps (calcination temperature). Thus, it leads to the generation of active sites with the change in physico-chemical properties.

18.3.1 Synthesis of mixed or composite metal oxides

The mixed or composite metal oxides can be prepared by various synthetic approaches namely coprecipitation, hydrothermal, solid state, sol-gel, and more [75]. The obtained material is considered as an intermediate, which upon calcination results in the

formation of mixed or composite metal oxide. By changing the synthetic approach and calcination temperature, the purity and physico-chemical properties of these materials can be modulated. Among the synthetic approaches, coprecipitation is found to be a suitable method to form homogeneous distribution of metal species components with a definite stoichiometry which can be easily converted into an active catalyst. It involves the precipitation of two or more metal salts simultaneously in a solution resulting in the formation of M_A–M_B hydroxide or M_A–M_B–M_C hydroxide which acts as an intermediate before calcination step. Upon calcination, the hydroxides undergo dehydroxylation leading to the formation of mixed [M_A–M_B–O_y] or composite metal oxides [M_A–M_B–O_y (mixed metal oxide) + M_AO + M_BO]. The factors affecting the material synthesis are the M_A to M_B mole ratio, pH of composition, concentration of precipitating agent, temperature, and aging period. The chemistry for the formation of mixed and composite oxide is represented in Scheme 18.3.

18.3.2 Chemical properties of mixed and composite metal oxides

Acid-base and redox properties as well as thermal and mechanical stabilities change upon the formation of mixed or composite metal oxides. Therefore, these are important class of materials for catalysis. Owing to the presence of $M^{n+}O^{n-}$ ion pairs in metal oxide, it is found to exhibit acid-base and redox properties. The generation of new and strong acid sites in mixed oxides has been ascribed to a charge imbalance localized in M_1-O-M_2 bondings where M_1 and M_2 are metal ions. This is partially attributed to the surface imperfections in crystallites. The imperfections in crystallites are metal or oxygen vacancies which cause a local charge imbalance. The existence of coordinatively unsaturated cations was responsible for the Lewis acidity. The extent of basicity (Lewis base) in these materials depends on the coordination number of oxygen species present in metal oxides, whereas the acidity (Lewis acid) is generated by the coordinatively unsaturated metal cations. The oxygen ions with low coordination number on the metal oxide are considered to be responsible for basicity [37, 65, 76–78]. The active sites in mixed or composite oxide are represented in Scheme 18.4. Also, a solid material with the combination of two catalytic functions is said to be a bifunctional catalyst.

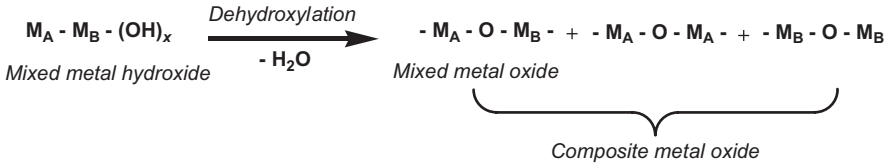

Scheme 18.3 Representation of the formation of composite metal oxides.

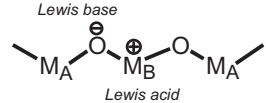

Scheme 18.4 Acidic and basic properties in mixed oxide.

18.3.3 Applications of composite tin oxides

Tin oxide-based materials have gained considerable attention in the recent years for their potential to facilitate both fundamental research and practical applications through their advantageous chemical and physical properties. There are several SnO_2-based mixed and composite metal oxides are reported for catalytic applications. These catalysts were highly active compared to that of individual metal oxides due to its excellent properties [30, 35, 79–87]. In this subtopic, some of these materials are discussed as follows.

18.3.3.1 Zn–Sn composite oxide as a bifunctional catalyst

Manjunathan et al. have reported the bifunctional Zn–Sn composite oxide as a highly active and selective catalyst to synthesize glycerol carbonate through carbonylation of glycerol with urea [80]. Glycerol carbonate has both direct and indirect applications in various fields owing to its interesting properties that lie in between cyclic alkylene carbonate and glycerol. In this work, Zn–Sn composite oxide catalysts were prepared by three different routes, namely, coprecipitation, solid-state, and solvent evaporation methods. Further, the properties in Zn–Sn composite oxide were altered by varying Zn-to-Sn molar ratio and calcination temperature.

The XRD patterns of Zn–Sn composite oxide prepared through solid state (SS) and solvent evaporation method (Evp), respectively, showed a main phase of ZnO and SnO_2 along with a little spinel crystalline phase of Zn_2SnO_4 in Fig. 18.4A. Conversely, Zn–Sn composite oxide prepared by coprecipitation method (CoPre) showed the main diffraction peak of spinel-structured Zn_2SnO_4 with the coexistence of ZnO and SnO_2 in Fig. 18.4B. The reason for the formation of Zn_2SnO_4 as the major component was explained as follows. The coprecipitation of Zn and Sn salts resulted in the formation of a perovskite-type Zn–Sn hydroxide as the intermediate before the calcination step [88]. Upon calcination to 600°C, Zn–Sn hydroxide undergoes dehydroxylation leading to the formation of Zn_2SnO_4 spinel [80].

Interestingly, the scanning electron microscopy analysis revealed that the variation in morphology and particle size depending upon the adopted catalyst preparation routes for Zn–Sn composite oxide as shown in Fig. 18.5. Zn_1Sn-CoPre-600 showed octahedral morphology containing an average particle size of 1.6 μm. Also, the change in Zn/Sn molar ratio prepared by the coprecipitation route resulted in a different morphology with varying particle size (Fig. 18.5C, D, and F). Zn_2Sn-CoPre-600 exhibited cubic shape with the average particle size was 1.6 μm whereas the Zn_3Sn-CoPre-600 possessed octahedral morphology containing an average particle size of 1.7 μm. Apart from that, there was some protuberance on the surface of octahedral or cubic morphology in all the Zn_xSn-CoPre-600 ($x = 1–3$) which could be caused by the growth of ZnO by the secondary nucleation from the excess of Zn species. As the Zn/Sn mole ratio increases from 2 to 3, the formation of ZnO from secondary nucleation masks the octahedral surface which is also confirmed from XRD by showing an increase of peak intensity corresponding to ZnO.

Importantly, the Zn–Sn composite oxide prepared through coprecipitation method showed a higher amount of acidity and basicity than the composite oxides prepared by

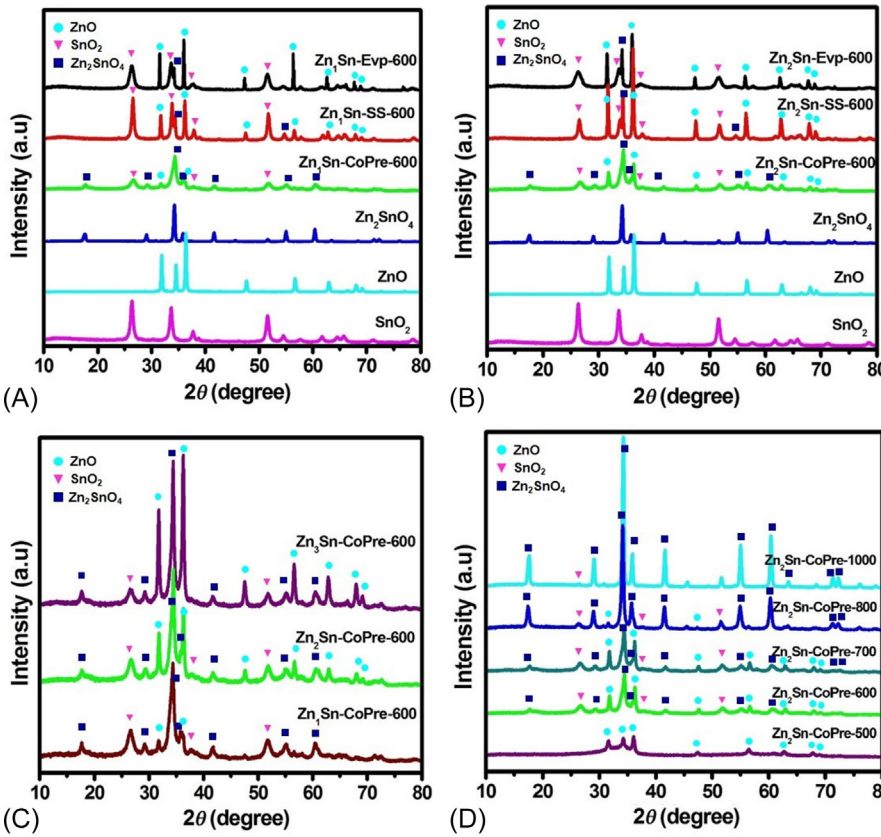

Fig. 18.4 XRD patterns of (A) individual and composite Zn−Sn oxides prepared by three different methods with Zn/Sn = 1; (B) Zn/Sn = 2; (C) effect of Zn/Sn molar ratio in Zn−Sn composite oxides; and (D) Zn_2Sn-CoPre catalysts prepared at different calcinations temperatures.

other preparation methods as tabulated in Table 18.3. The total acidity and basicity of catalysts prepared by different methods decreased in the order: coprecipitation > solid state > solvent evaporation. The generation of greater active sites by coprecipitation approach was attributed to the uniformity in forming Zn-O-Sn bonding in greater extent compared to other approaches as the presence of Zn_2SnO_4 spinel phase was higher for calcined Zn-Sn-hydroxide prepared by coprecipitation. The presence of greater amount of Zn_2SnO_4 phase could be a reason for greater acidity. This is also confirmed by higher acidity of individual Zn_2SnO_4 compared with ZnO and SnO_2.

The catalytic behavior of Zn−Sn composite oxides prepared through different routes was evaluated for the carbonylation reaction of glycerol with urea (shown in Scheme 18.5.) and the results are tabulated in Table 18.3. The pure oxides namely ZnO, SnO_2, and Zn_2SnO_4 showed moderate activity of 66.4%, 39.6%, and 50% glycerol conversion with glycerol carbonate selectivity of 98%, 99%, and 96%, respectively. The Zn−Sn composite oxides exhibited higher catalytic activity than the

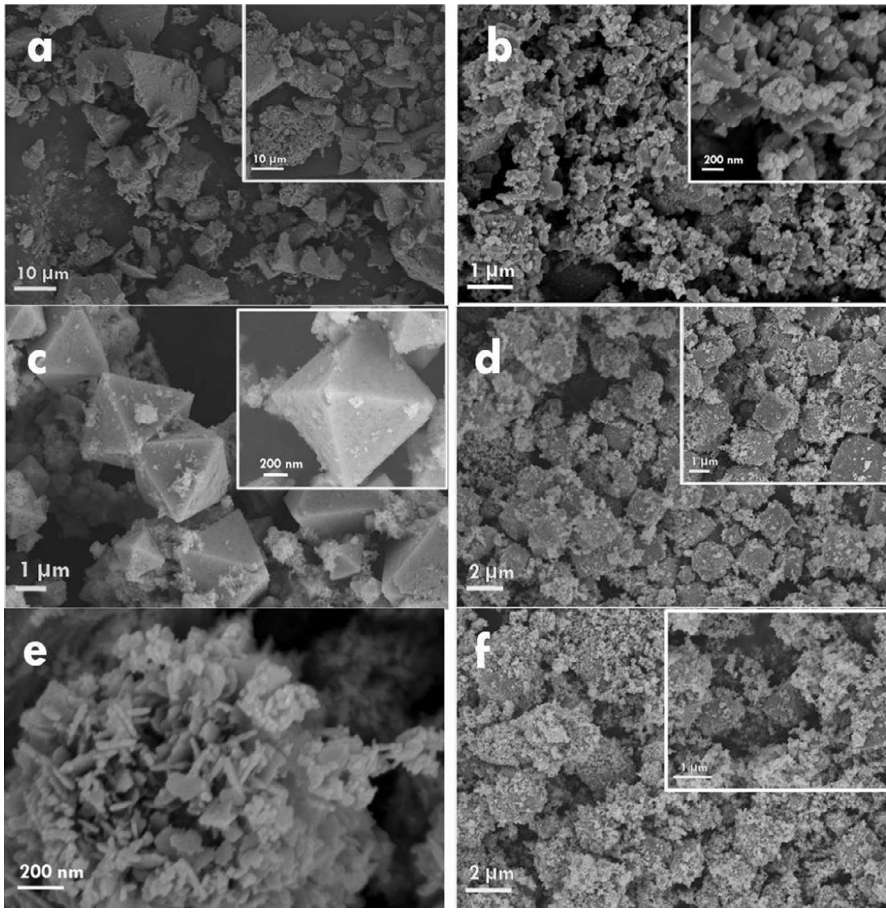

Fig. 18.5 SEM images for (A) Zn_1Sn-Evp-600, (B) Zn_1Sn-SS-600, (C) Zn_1Sn-CoPre-600, (D) Zn_2Sn-CoPre-600, (E) Zn_2Sn-CoPre-600 (secondary nucleation on cubic surface), and (F) Zn_3Sn-CoPre-600.
Reprinted with permission from Manjunathan P, Ravishankar R, Shanbhag GV. ChemCatChem 2016;8:631–639. Copyright (2016) John Wiley and Sons.

individual oxides. Among the composite oxides, catalyst preparation procedure influenced greatly the catalytic performance. Zn_1Sn-CoPre-600 catalyst gave highest glycerol conversion of 88% with approximately 99% selectivity for glycerol carbonate. The superior catalytic activity of Zn_1Sn-CoPre-600 was mainly attributed to the presence of higher amount of active sites, that is, both acidic and basic sites (shown in Table 18.3). The lower activities of ZnO, SnO_2, and Zn_2SnO_4 compared to that of the composite oxides are mainly caused by the lower amount of active sites present in the catalysts. The glycerol carbonate yield over Zn_1Sn catalysts prepared through different routes decreased with decrease in the amount of active sites in the following trend: Zn_1Sn-CoPre-600 > Zn_1Sn-SS-600 > Zn_1Sn-Evp-600.

Table 18.3 Physico-chemical properties and catalytic activities of individual metal oxides and Zn-Sn composite oxides–[80]

Catalyst	Calcination temp (°C)	S_{BET}[a] (m^2/g)	Acidity (μmol NH_3/g)[b]	Basicity (μmol CO_2/g)[c]	Total active sites (μmol/g)[d]	Gly Conv. (wt%)[e]	Glycerol carbonate (wt%)[e]	
							Selec.	Yield
Blank	–	–	0	0	0	32.0	95.8	30.6
ZnO	600	18.9	60	12	72	66.4	98.1	65.1
SnO_2	600	16.6	30	4	34	39.6	99.0	39.2
Zn_2SnO_4	600	40.0	160	20	180	50.0	96.0	48.0
Zn_1Sn-CoPre	600	13.3	235	52	287	88.0	99.2	87.3
Zn_2Sn-CoPre	600	15.2	268	61	329	96.0	99.6	95.6
Zn_3Sn-CoPre	600	17.0	256	48	304	90.7	98.7	89.5
Zn_1Sn-SS	600	8.9	216	38	254	79.5	99.4	79.0
Zn_2Sn-SS	600	9.2	223	45	268	84.0	99.2	83.3
Zn_1Sn-Evp	600	31.5	181	35	216	76.1	99.2	75.5
Zn_2Sn-Evp	600	33.2	210	48	258	80.0	99.0	79.2
Zn_2Sn-CoPre	500	25.0	207	30	237	*	*	*
Zn_2Sn-CoPre	600	15.2	268	61	329	96.0	99.6	95.6
Zn_2Sn-CoPre	700	14.1	240	53	293	*	*	*
Zn_2Sn-CoPre	800	6.0	155	27	182	*	*	*
Zn_2Sn-CoPre	1000	3.0	100	7	107	*	*	*

[a] BET surface area,
[b] NH_3-TPD,
[c] CO_2-TPD,
[d] Total active sites = sum of acidity and basicity,
[e] **Reaction conditions:** glycerol = 2 g, urea = 1.31 g, catalyst = 0.33 g, reaction temperature = 155°C, time = 4 h, under N_2 bubbling,
* Result is shown in Fig. 18.6.

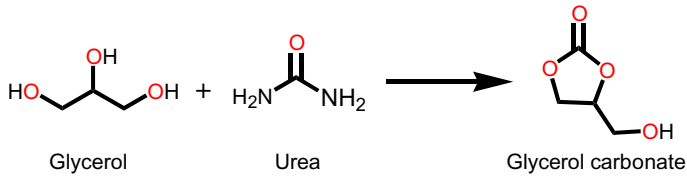

Scheme 18.5 Carbonylation of glycerol with urea

The effect of Zn/Sn molar ratio from 1 to 3 showed a substantial improvement in glycerol conversion from 88% (Zn_1Sn-CoPre-600) to 96% (Zn_2Sn-CoPre-600) with glycerol carbonate selectivity of ≥99% as shown in Table 18.3. Further increase of Zn content from 2 to 3 (Zn_3Sn-CoPre-600) showed a marginal decrease of glycerol conversion by approximately 5%. The greater catalytic activity of Zn_2Sn-CoPre-600 catalyst was attributed to the presence of higher amount of active sites than for other catalysts. Moreover, the catalysts prepared by the other two methods with best composition of Zn/Sn = 2, that is, Zn_2Sn-SS-600 and Zn_2Sn-Evp-600, showed lower catalytic activity (84% and 80% conversion, respectively) than Zn_2Sn-CoPre-600 owing to the presence of lower amount of active sites.

In addition to this, the effect of calcination temperature of Zn_2Sn-CoPre was studied by varying the calcination temperature ranging from 500°C to 1000°C and the results are depicted in Fig. 18.6. Upon increasing of calcination temperature from 500°C to 600°C, the glycerol conversion increased appreciably (from 88.5% to 96%) along with an increase in glycerol carbonate selectivity (98.5%–99.6%). However, by further increasing the calcination temperature from 600°C to 1000°C, showed a considerable

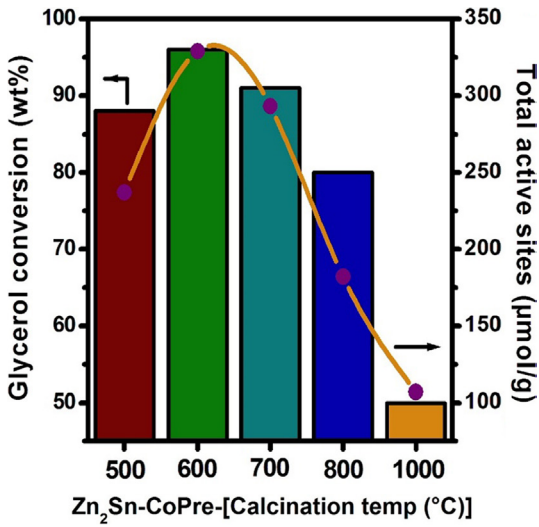

Fig. 18.6 Effect of calcination temperature on catalytic activity. **Reaction conditions:** glycerol (2 g), urea (1.31 g), catalyst (0.33 g), reaction temperature = 155°C, and time = 4 h, under N_2 bubbling.

decrease in glycerol conversion from 96% to 50% due to the decrease in total active sites from 329 to 107 µmol/g. Also, the decrease in active sites upon increase of calcination temperature could be attributed to the decrease of surface area owing to the agglomeration of particles resulting in less surface metal-oxygen pairs [89].

18.3.4 Applications of mixed metal oxides

18.3.4.1 Tin-Tungsten mixed oxide for C–C bond-forming reactions

WO_3-SnO_2 possesses strong acid sites and shows high activities for various types of acid-catalyzed reactions. WO_3-SnO_2 has been utilized for some organic syntheses such as cyclization of citronellal, Diels-Alder reactions, cyanoethylation, hydration of aldoximes to nitriles, hydration of alkynes, carbonylation of glycerol, and isomerization of glucose and fructose [35, 79, 81, 83, 84, 90].

Mizuno and co-workers reported the catalytic behavior of tin-tungsten mixed oxide for few important reactions namely cyclization of citronellal, Diels-Alder reactions, and the cyanosilylation of carbonyl compounds with trimethylsilyl cyanide (TMSCN), hydration of alkynes, and isomerization of glucose and fructose [35, 81, 84]. Here, the work on cyclization of citronellal is discussed in detail. In this study, two decisive parameters were varied namely Sn-to-W mole ratio and calcination temperature. The Sn–W oxides were obtained by calcining SnW-hydroxide precursor which was prepared from coprecipitation of Sn and W salts. The authors claim that the Brønsted acid sites generated on the aggregated polytungstate species on SnW2–800 likely play an important role in the C–C bond-forming reactions [35].

The Sn–W oxide with the Sn/W molar ratio of *x* calcined at *T*°C is designated as SnW*x*–*T*. These catalysts were evaluated for the cyclization of (*R*)-(+)-citronellal **(1)** which shows a complex selectivity pattern since it forms four different diastereoisomers products (Scheme 18.6 **2a**–**2d**) and results are shown in Table 18.4. Importantly, it showed no reaction in the absence of a catalyst (entry 1), or in the presence of SnO_2 (entry 2), or WO_3 (entry 3), or a mixture of SnO_2 and WO_3 (entry 4). The catalyst precursor, that is, Sn–W hydroxide was not active for the present cyclization (entry 5). Among the SnW*x*–*T* catalysts, SnW2–800 showed the highest catalytic activity for the cyclization of (*R*)-(+)-citronellal (1) (entry 11). The catalytic activity of SnW2–800 was much higher than that of acid-type zeolites such as H-MOR and H–Y (entries 16 and 17).

From the literature, it is shown that a high diastereoselectivities in favor of **2a** (>70%) is formed in the presence of Lewis acidic sites. With Brønsted acids, the diastereoselectivities are typically lower, which is in the range of 50%–70% than those

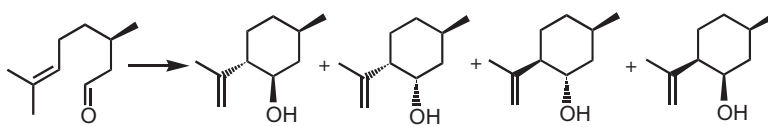

Scheme 18.6 Cyclization of citronellal

Table 18.4 Physico-chemical properties and catalytic activities of various catalysts for cyclization of citronellal

Entry	Catalyst	Sn/W	BET surface area (m^2/g)	Amount of acidic site[a] (μmol/g)	Brønsted acid site[b] (μmol/g)	Ratio of Brønsted/ Lewis acid site[a] %	Conv. (%)	Selec. (%)	Isomer ratio				R [mmol/ min/g]
									2a	2b	2c	2d	
1	none	–	–	–	–	–	nr	–	–	–	–	–	–
2	SnO_2	–	–	–	–	–	nr	–	–	–	–	–	–
3	WO_3	–	–	–	–	–	nr	–	–	–	–	–	–
4	$SnO_2 + WO_3$[c]	1	–	–	–	–	nr	–	–	–	–	–	–
5	Sn-W hydroxide	2	–	–	–	–	nr	–	–	–	–	–	–
6	SnW1.5–400	1.5	134	303	134	44/56	12	93	59	35	4	2	0.53
7	SnW1.5–600	1.5	103	219	127	58/42	25	94	57	37	4	2	0.72
8	SnW1.5–800	1.5	77.4	124	82	66/34	86	90	58	38	3	1	6.9
9	SnW2–400	2	143	290	124	43/57	12	95	59	35	4	2	0.26
10	SnW2–600	2	118	189	102	54/46	46	94	59	37	3	1	1.6
11	SnW2–800	2	73.6	134	97	73/27	95	93	58	38	3	1	8.7
12	SnW2–1000	2	29.5	27	–[d]	–[d]	4	92	62	35	3	<1	0.024
13	SnW1–800	1	35.8	73	43	58/42	28	89	60	36	3	1	0.74
14	SnW5–800	5	68.8	78	–[d]	–[d]	69	90	58	38	3	1	3.7
15	SnW10–800	10	49.4	55	–[d]	–[d]	30	91	59	38	3	1	1.1
16	H-MOR	–	–	–	–	–	6	94	61	35	3	1	0.094
17	H-Y	–	–	–	–	–	8	84	67	29	3	1	0.10

[a] Amount of acidic sites were determined from NH_3-TPD measurement.
[b] Amount of Brønsted acid sites were determined from IR spectra of pyridine adsorbed on the Sn−W oxides.
[c] A mixture of SnO_2 (5 mg) and WO_3 (5 mg).
[d] IR spectra of pyridine adsorbed on the Sn−W oxides did not measured because the transmittance was almost 0%. Reaction conditions: 1 (1 mmol), catalyst (10 mg), dichloromethane (5 mL), 20°C, 1 h. Conversion and selectivity were determined by GC analysis, nr = no reaction.

with Lewis acids. Using Sn–W oxides, the diastereoselectivities in favor of **2a** were 58%–62% (Table 18.1) and these values were in good agreement with those obtained for Brønsted acid catalysts [91–94].

To clarify the active sites of Sn–W oxides for the cyclization, the authors studied the reaction in the presence of 2,6-lutidine. It is well known that 2,6-lutidine can selectively interact with Brønsted acid sites and cannot interact with Lewis acid sites due to the steric hindrance [95]. Fig. 18.7 shows the dependence of the reaction rates of SnW2–800 and SnW2–400 on the amounts of 2,6-lutidine added. The reactions with SnW2–800 and SnW2–400 were almost completely inhibited by the presence of equimolar amounts of 2,6-lutidine with respect to those of Brønsted acid sites (97 and 124 μmol/g, respectively). Upon addition of 2,6-lutidine (30 μmol/g), the reaction rates for SnW2–800 significantly decreased by 93%, whereas for SnW2–400, the rates gradually decreased by 40%. The reaction rate for SnW2–600 gradually decreased by 20% upon the addition of 2,6-lutidine (30 μmol/g), and the reaction was completely inhibited by the presence of the equimolar amount of 2,6-lutidine with respect to that of the Brønsted acid sites (102 μmol/g). All these results show that the cyclization of (*R*)-(+)-citronellal is mainly promoted by the Brønsted acid sites present in Sn–W oxides, and that SnW2–800 possesses strong Brønsted acid sites [35].

18.4 Tin oxide as a catalyst support

18.4.1 Metal oxide supported on SnO_2 as an acid and base catalyst

Tin oxide (SnO_2) has been used as a potential catalyst support in catalysis due to its stability and durability. SnO_2 is used as a catalyst support by impregnating anion or cation [M/SnO_2 (M = Ca, Si, WO_3, MoO_3, Pd, and more) HPA/SnO_2, SO_4^{2-}/SnO_2] on

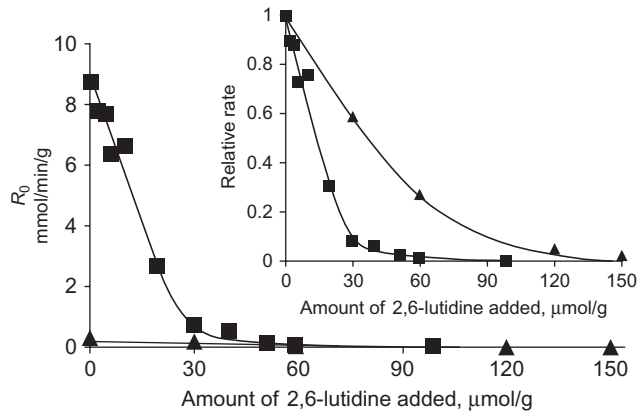

Fig. 18.7 The dependence of the reaction rates of SnW2–800 (&) and SnW2–400 (~) on the amounts of 2,6-lutidine added for the cyclization of 1. (Inset: The dependence of the relative rates on the amounts of 2,6-lutidine added. The rates in the absence of 2,6-lutidine were taken as unity.)
Reprinted with permission from Ogasawara Y, Uchida S, Yamaguchi K, Mizuno N. Chem A Eur J 2009;15:4343–4349. Copyright (2016) John Wiley and Sons.

the catalyst surface followed by activation through calcination to generate active sites which is used for various organic reactions [29, 30, 96–100].

18.4.1.1 CaO/SnO_2

Calcium oxide (CaO) and tungsten oxide (WO3) supported on tin oxide was reported by Xie and co-workers for transesterification of soybean oil [82, 101]. CaO has been revealed as a promising solid base catalyst for the synthesis of biodiesel at mild temperatures and at atmospheric pressure. However, CaO undergoes leaching by dissolution of the solid in the reaction medium [102]. The first aspect affects the industrial application as extensive leaching of active sites may threaten the reusability and the environmental sustainability of catalyst [103]. To improve the performance of calcium-based catalysts, the CaO-supported acidic oxide catalysts are expected to enhance the catalyst stability by reducing the leaching of catalyst due to the interaction between CaO and the other acidic oxides in the solid catalyst.

In this work, a solid CaO supported on SnO_2 catalyst was prepared by incipient wetness impregnation method. The required concentration of calcium nitrate [$Ca(NO_3)_2$] was impregnated on tin hydroxide powder [$Sn(OH)_4$] followed by calcination at a desired temperature and was used as a heterogeneous catalyst for the transesterification of soybean oil with methanol. From XRD analysis, it is found that the compound consists of three different oxides namely CaO, SnO_2, and $CaSnO_3$ as depicted in Fig. 18.8. It was proposed that the stability of the CaO catalyst could be improved by using acidic SnO_2 as support. This is due to the substitution of Sn ions by Ca ions with the

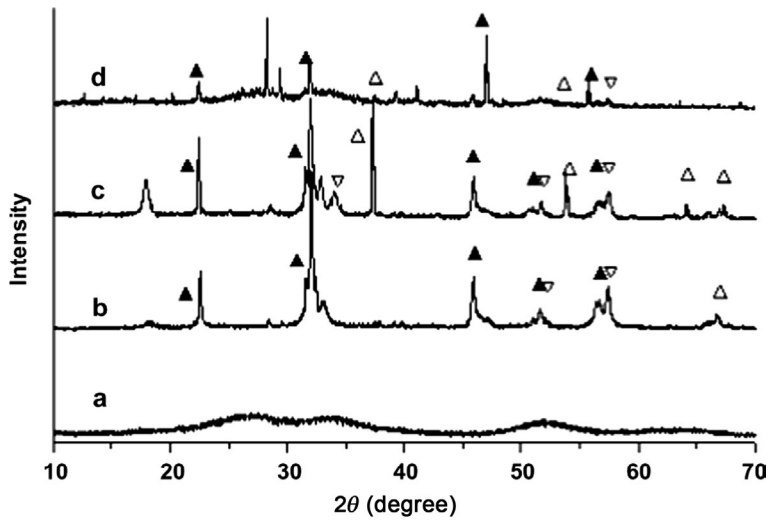

Fig. 18.8 XRD patterns for CaO-SnO_2 catalysts with different Ca/Sn ratios. (A) $Sn(OH)_4$ powder; (B) Ca/Sn 2:1; (C) Ca/Sn 4:1; and (D) Ca/Sn 6:1. The calcination temperature is 700 °C. (△)CaO; (▽)SnO_2; and (▲)$CaSnO_3$.
Reprinted with permission from Xie W, Zhao L. Energ Conver Manage 2013;76:55–62.

Table 18.5 Influence of preparation conditions on the catalytic activity of the solid catalyst [101]

Entry	Calcination temperature (°C)	Ca/Sn molar ratio	Conversion (%)
1	500	4:1	43.1
2	600	4:1	70.5
3	700	4:1	89.3
4	800	4:1	85.4
5	900	4:1	84.7
6	700	2:1	50.3
7	700	3:1	74.6
8	700	4:1	89.3
9	700	5:1	83.5
10	700	6:1	76.4

Reaction conditions: methanol: oil molar ratio = 12:1, catalyst amount = 8 wt%, reaction temperature = 65°C, reaction time = 6 h.

formation of $CaSnO_3$ results in the electron transfer between the catalyst components. With this interaction, the leaching of catalyst components could be reduced leading to an enhanced stability of the solid catalyst. Upon calcination of CaO-supported SnO_2 catalyst, the acid-base interaction between the basic CaO and the acidic SnO_2 would provide a high dispersion of the catalytically active sites which ultimately improves the stability of the solid catalyst [104]. The effect of Ca/Sn ratio and calcination temperature on the catalytic activity was investigated for the conversion of soybean oil to methyl esters. The catalytic activity was found to be highly dependent on the Ca/Sn ratio and calcination temperature as depicted in Table 18.5. The catalyst with Ca/Sn molar ratio of 4:1 calcined at a temperature of 700°C exhibited best activity by reaching the conversion of 89.3%.

18.4.1.2 WO_3/SnO_2

In another work, Xie and coworkers [82] reported the transesterification of soybean oil with methanol to fatty acid methyl ester (FAME) using WO_3/SnO_2 solid as a heterogeneous acid catalyst. In this study, the authors determined the effect of catalyst preparation parameters by impregnating different metal oxides (WO_3, MoO_3, and TiO_2) on various supports such as SnO_2, Al_2O_3, and ZrO_2. The individual metal oxides namely WO_3, SnO_2, and ZrO_2 gave lower conversion of soybean oil; 32.4%, 22.1%, and 10.5%, respectively, due to the presence of weak acidity as shown in Table 18.6. However, upon loading the metal oxides on the supports and activation at a high temperature improved their catalytic activity. Among the catalysts screened, the solid acids such as WO_3/SnO_2, TiO_2/SnO_2, TiO_2/Al_2O_3, WO_3/ZrO_2, TiO_2/ZrO_2, and MoO_3/ZrO_2 were shown to have the catalytic activity greater than 50% over other investigated catalysts. In particular, the WO_3/SnO_2 showed the best catalytic activity achieving a conversion of 79.1%. It is expected that the incorporation of tungstate oxides on SnO_2

Table 18.6 Influence of preparation conditions on the catalytic activity of the solid catalyst [82]

Entry	Catalysts	Calcination temperature (°C)	Conversion (%)
1	WO_3	600	32.4
2	ZrO_2	600	10.5
3	SnO_2	600	22.1
4	WO_3/Al_2O_3	600	45.5
5	MoO_3/Al_2O_3	600	46.8
6	TiO_2/Al_2O_3	600	58.8
7	WO_3/ZrO_2	650	65.4
8	MoO_3/ZrO_2	500	62.8
9	TiO_2/ZrO_2	600	63.2
10	WO_3/SnO_2	900	79.1
11	MoO_3/SnO_2	600	51.6
12	TiO_2/SnO_2	900	61.2

Reaction conditions: methanol: oil molar ratio = 30:1, catalyst amount = 5 wt%, reaction temperature = 180°C, reaction time = 5 h.

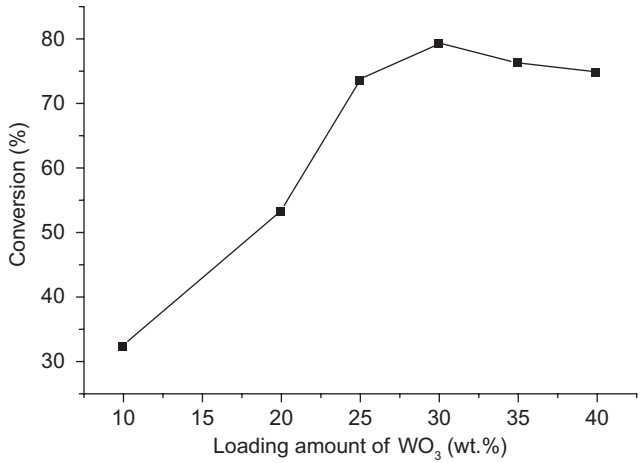

Fig. 18.9 Influence of WO_3 loading amount on the activity of the catalyst. Reaction conditions: catalyst amount 5 wt%, reaction time 5 h, reaction temperature 180°C, and methanol/oil molar ratio 30:1.
Reprinted with permission from Xie W, Wang T. Fuel Process Technol 2013;109:150–155. Copyright (2016) Elsevier.

leads to the formation of higher number of acidic sites in comparison with that of SnO_2 which could be the reason for greater activity. Also, the oil conversion was found to be gradually improved from 32.3% to 79.2% upon increasing WO_3 loading from 10 to 30 wt% as represented in Fig. 18.9. However, the catalytic activity was not appreciable with further increase in the WO_3 loading ≥35 wt%. Overall, the WO_3/SnO_2 catalyst

with WO_3 loading of 30% and calcined at 900°C showed the best catalytic performance. The maximum conversion to FAME of 79.2% was achieved after 5 h at 110°C with 30:1 mole ratio of methanol to oil and 5 wt% of catalyst. The authors also claimed that the solid acid catalyst was reused for four runs without significant deactivation.

18.4.1.3 Heteropoly acid supported on SnO_2 as an acid catalyst

Heteropolyacids (HPAs) have attracted a lot of attention as an efficient acid catalyst due to its remarkable advantages, such as strong Brønsted acidity, thermal stability, unique structure, surface charge distribution, and environmental friendliness [105–107]. However, the major disadvantages of HPAs, as catalyst lies in their low surface area ($<10\,m^2/g$), and high solubility in polar solvents and separation problems from reaction mixture [99]. HPAs can be heterogenized by exchanging its protons (H^+) with metal ions [108–112] and/or supporting them on a suitable support [99, 113–119]. The acidity and catalytic activity of supported HPAs depend on the type of the supports, the HPA loading, pretreatment conditions, etc. The catalyst support plays an important role in enhancing the acidity, thermal stability, and surface area of the final catalyst [105, 120].

HPA supported on variety of supports are studied as catalysts for various organic transformation reactions. In this section, we focus on HPA supported on SnO_2 as a catalyst. Lingaiah and Ahmed co-workers have studied HPA supported on SnO_2 for variety of reactions namely benzylation of anisole [116], glycerol etherification [120], esterification of free fatty acids [117], esterification of amyl alcohol [115], Pechmann reaction [99], etc.

They investigated 12-tungstophosphoric acid (TPA) supported on SnO_2 for benzylation of anisole with benzyl alcohol [116]. In this work, a series of TPA supported on tin oxide (TPA-SnO_2) catalysts with varying TPA content was prepared by wet impregnation technique followed by calcination at 300°C. These catalysts were characterized by FTIR, X-ray diffraction, laser Raman spectroscopy, and NH_3-TPD. The FTIR patterns of TPA supported on SnO_2 catalysts showed four bands in the region of 1100–500 cm^{-1} and depicted in Fig. 18.10. The main bands at 1081, 986, 890, and 800 cm^{-1} are assigned to the stretching vibrations of P–O, W=O_t, W–O_c–W, and W–O_e–W, respectively, related to Keggin ion which indicates that the Keggin structure of heteropoly tungstate remained unaltered on SnO_2 support. The XRD patterns of the catalysts suggest the presence of tetragonal cassiterite structure of SnO_2 is shown in Fig. 18.10. The XRD results suggest that TPA is well dispersed on SnO_2 at low content of TPA. The TPA loaded above 15 wt% showed weak peaks related to Keggin structure. The NH_3-TPD analysis of the catalysts showed three types of acid strengths and results are presented in Table 18.7. The amount of acidity was increased by increasing the amount of TPA until 20% TPA/SnO_2. However, the acid strength varies by varying the TPA content on SnO_2 and suggests the presence of strong acid sites for the catalyst with 15 wt% of TPA.

The catalytic activities of TPA/SnO_2 catalysts were evaluated for benzylation of anisole with benzyl alcohol as benzylating agent (Scheme 18.7) and the results are shown in Table 18.8. The bare SnO_2 showed negligible activity for the benzylation

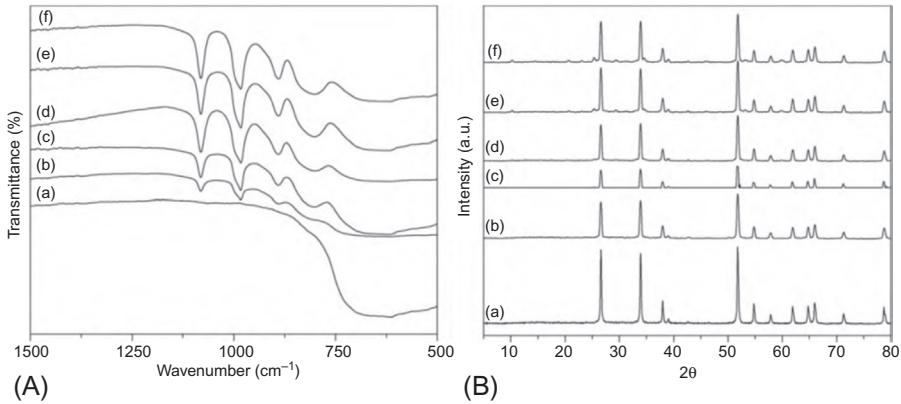

Fig. 18.10 **(A)** FTIR spectra of heteropoly tungstate supported on tin oxide catalysts and **(B)** XRD patterns of heteropoly tungstate supported on tin oxide catalysts. (a) SnO_2, (b) 5% TPA/SnO_2, (c) 10% TPA/SnO_2, (d) 15% TPA/SnO_2, (e) 20% TPA/SnO_2, and (f) 25% TPA/SnO_2. Reprinted with permission from Kumar CR, Prasad PS, Lingaiah N. Appl Catal Gen 2010;384:101–106. Copyright (2016) Elsevier.

Table 18.7 Acid strength distribution of TPA/SnO_2 by NH_3-TPD [116, 117]

Catalyst	Surface area (m^2/g)	Acidity (μmol/g)			
		Weak	Moderate	Strong	Total
SnO_2	15.1	–	–	–	–
5%TPA/SnO_2	14.0	58	–	49	107
10%TPA/SnO_2	13.1	9	48	30	87
15%TPA/SnO_2	11.8	–	75	56	131
20%TPA/SnO_2	11.6	–	96	37	133
25%TPA/SnO_2	11.5	–	89	31	120

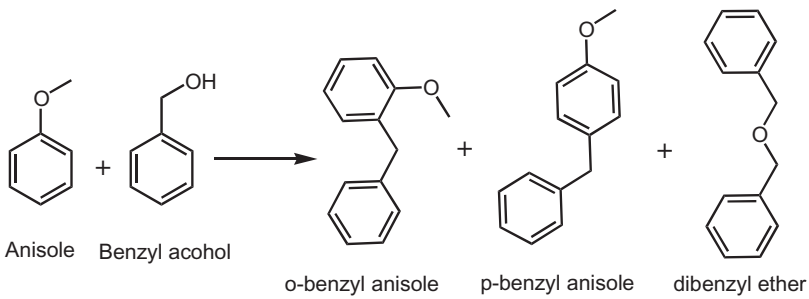

Scheme 18.7 Benzylation of anisole with benzyl alcohol

Table 18.8 Effect of TPA loading on tin oxide on the benzylation of anisole [116]

Catalyst	Benzyl alcohol conversion (%)	Yield (%)		
		ortho-	para-	Ether
SnO_2	1.6	0.5	0.6	0.5
5%TPA/SnO_2	14.1	3.8	4.6	5.7
10%TPA/SnO_2	85.2	27.6	34.0	23.6
15%TPA/SnO_2	95.1	34.0	39.7	21.5
20%TPA/SnO_2	89.2	22.9	36.7	22.6
25%TPA/SnO_2	95.1	31.9	40.2	23.0

Reaction conditions: Anisole (10 g), benzyl alcohol (3.376 g), catalyst weight (0.1 g), reaction temp = 120 °C, reaction time = 1.5 h.

of anisole. The reaction with TPA supported on SnO_2 resulted in increase of catalytic activity as a function of active component loading, reached to a maximum for the catalyst with 15 wt% TPA, and remained almost constant with further increase. The activity was correlated with the strength and amount of acidity. The greater activity of 15% TPA/SnO_2 catalyst was due to strong acidic sites with high amount of total acidity, as shown in Table 18.8. A similar activity at high TPA content was attributed to the presence of the same amount of total acidity. These results suggest that moderate to strong acidic sites are responsible for benzylation activity. Thus, the benzylation of anisole is dependent on the acidity of the catalyst, which depends on the dispersion and retention of Keggin ions of TPA on the support.

18.5 Photocatalysis application of tin oxide-based materials

Tin oxide nanomaterials play a vital role for photocatalytic applications namely degradation of a number of common textile dyes and organic compounds and hydrogen generation reactions. Bhattacharjee and co-workers [121–124] reported degradation of a variety of common textile dyes like eosin Y, rose bengal, methylene blue, and methyl violet 6B by employing direct sunlight as a source. The utilization of sun light is found to be a very cost-effective approach which could be scalable to a large extent compared to common UV-assisted photodegradation technique. The recombination of photogenerated electrons and holes is disadvantageous for efficient photocatalytic activity. Therefore, the anti-recombination of carriers can be endorsed by modifying tin oxide nanostructures with methods like cation/anion doping, composite formation, and impregnation on different supports.

Pan et al. [125] reported that the indium tin oxide nanoparticles show higher photodegradation efficiency of rhodamine B than the commercial P25 TiO_2 within the given concentration range. Further, Sinha and co-workers [126] investigated the light-assisted degradation of a variety of dyes namely methylene blue, malachite green, methyl violet, methyl green, rhodamine B, and rose bengal using Sn-SnO_2 NPs

and claimed that the presence of Sn(0) nanoparticles in spherical SnO_2 improves the charge (electrons and holes) separation efficiency thereby enhancing the rate of degradation. Sundaram and co-workers [127] have reported SnO_2-Ta_2O_5 composite for visible light photocatalytic degradation of methylene blue. This study showed that the SnO_2-Ta_2O_5 composite exhibited lower band gap compared with that of the individual SnO_2 and Ta_2O_5 and which could be due to the formation of a heterostructure. As a result, the SnO_2-Ta_2O_5 composite exhibited enhanced photocatalytic activity than the individual oxides to degrade methylene blue.

Few studies [128–130] have found that the doping of Sn^{2+} cations into the bulk of wide-band semiconducting oxides can extend the optical response of the materials into visible light region. Wang and co-workers [131] reported the tuning of valence band structure of SnO_2 by doping Sn^{2+} cations into bulk of SnO_2 nanoparticles. The study by combining the density functional theory (DFT) calculations and electrochemical analysis showed that the Sn^{2+} dopant induced the visible-light photocatalytic activity for H_2 production from ethanol (3.75%) in water solution. The flat-band potential observed from Mott-Schottky plots for SnO_2 samples suggests that the doping does not alter the conduction band energy level of nanocrystalline SnO_2 particles. It is deduced that the narrowed band gap could be originated from the formation of an impurity energy level in the valence band and it was also supported by the DFT studies. The Sn^{2+}-doped SnO_2 catalysts exhibited higher performance in photocatalytic reforming of ethanol for H_2 evolution reaction as shown in Fig. 18.11. Notably, the commercial SnO_2 and SnO were used for comparison and it showed no H_2 evolution under the identical reaction conditions. This provides a strong evidence that the enhanced photocatalytic activity at visible light region is attributed to the doping strategy. However, there was a significant deactivation observed for the active catalysts due to the oxidation of Sn^{2+} dopant into Sn^{4+} by the accumulative photogenerated holes.

Manikandan et al. [132] reported a mixed-valence tin oxide (Sn_3O_4) as a photocatalyst for water splitting under visible light using pure platinum (Pt) as a co-catalyst. The Sn_3O_4 material significantly catalyzed water splitting in aqueous solution under irradiation of visible light ($\lambda > 400$ nm), whereas none of the stable tin oxides, SnO and SnO_2, was active toward the reaction and the results are shown in Fig. 18.12. Further studies on theoretical calculations have revealed that the enhanced activity of Sn_3O_4 was attributed to the coexistence of Sn^{2+} and Sn^{4+}, resulting in a desirable band gap and band-edge position for the reduction of water in visible light.

18.6 Photoelectrocatalysis applications of tin oxide-based materials

Over the past decades, photoelectrocatalytic (PEC) pollutant degradation and water splitting have attracted significant attention for the purpose of environmental protection and clean energy production [133]. PEC water splitting provides a promising approach to convert sunlight into sustainable hydrogen energy [134]. Tin oxide (SnO_2) has received a great deal of attention as a photoanode because of its favorable energy-level

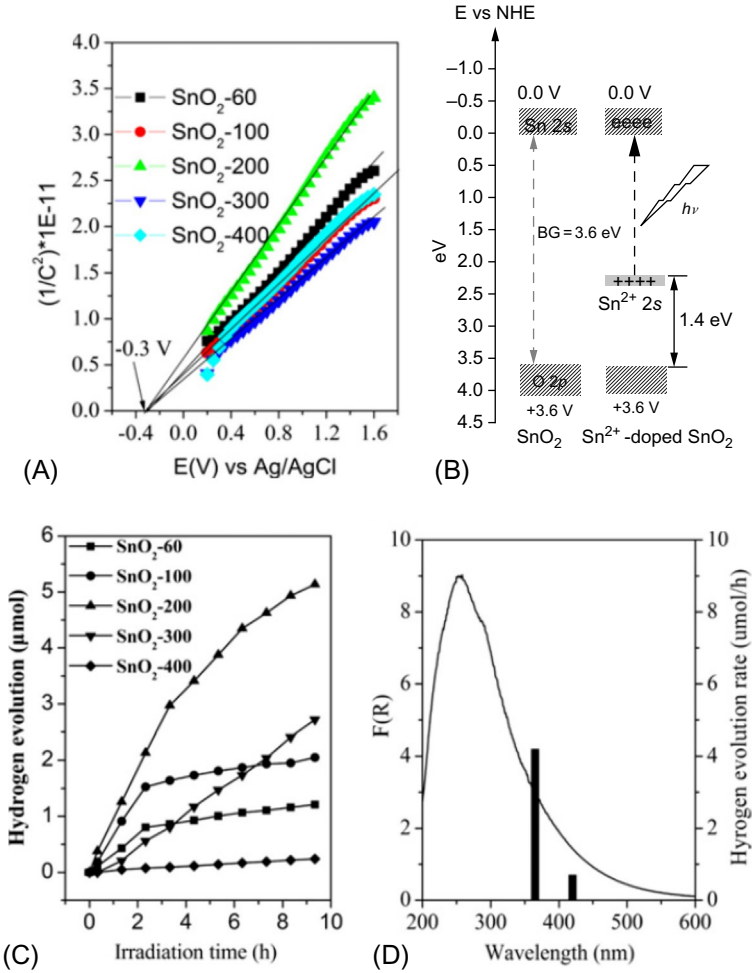

Fig. 18.11 (A) Mott-Schottky plot of the as-prepared SnO_2 samples; (B) the band structure of Sn^{2+}-doped SnO_2 photocatalysts; (C) time course of evolved H_2 over the as-prepared SnO_2 catalysts under visible light (≥420 nm) irradiation, and (D) wavelength dependence of hydrogen production on the SnO_2–500 catalyst.
Reprinted with permission from Long J, Xue W, Xie X, Gu Q, Zhou Y, Chi Y, Chen W, Ding Z, Wang X. Catal Commun 2011;16:215–219. Copyright (2011) Elsevier.

position, high photoactivity, excellent photocorrosion resistance, chemical stability, electron transport properties, and low cost [135]. All of these properties in SnO_2 made it beneficial for catalysis and sensing. However, to further promote the performance of SnO_2 in the field of catalysis, particularly for PEC applications, few barriers must be overcome. The first problem is its relatively large band gap, ∼3.5 eV, which limits its photoresponse to visible light; the second, fast recombination of electron-hole pairs in SnO_2, and the third, recycling problem of catalysts in powder form.

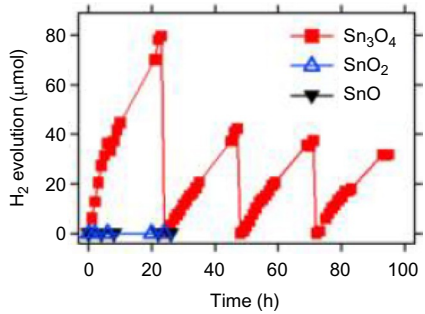

Fig. 18.12 Photocatalytic H_2 evolution from the aqueous methanol solution over SnO *(black triangles)*, SnO_2 *(blue triangles)*, and Sn_3O_4 *(red squares)* with 0.5 wt% Pt loading under the irradiation visible light (300 mg catalyst, $\lambda > 400$ nm).
Reprinted with permission from Manikandan M, Tanabe T, Li P, Ueda S, Ramesh GV, Kodiyath R, Wang J, Hara T, Dakshanamoorthy A, Ishihara S. ACS Appl Mater Interfaces 2014;6:3790–3793. Copyright (2014) ACS.

To overcome these limitations, various strategies have been employed, such as doping with metal and nonmetal ions, modification with noble metals, combination with narrow band gap semiconductors to build hybrid structures, and fabrication of recyclable films with superior optical, optoelectronic, and electronic properties [133].

Zhang et al. [133] studied the SnO_2@MoS_2 nanohybrids as a PEC material for the degradation of rhodamine B dye and water splitting reactions, and the results are shown in Fig. 18.13. In this study, the SnO_2@MoS_2 hybrid film was fabricated through an electrophoretic deposition method to promote PEC efficiency and to solve the recovery problem. Compared to the pure SnO_2 and MoS_2 films, the SnO_2@MoS_2 hybrid film exhibited enhanced PEC activities of pollutant degradation and water splitting. The enhancement was mainly ascribed to (a) the formation of high-quality SnO_2@MoS_2 heterostructures which improved the absorption efficiency of visible light and decreased the rate of the photoelectron-hole pair recombination, (b) the well-defined three-dimensional (3D) hierarchical morphology provided a large surface area, abundant active edge sites, and defects on the basal surfaces, and (c) the apparent synergetic effect between photo- and electrocatalysis facilitated charge generation, separation, and transfer.

In addition to this, Yin and his co-workers [136] developed a tree-like ZnO/TiO_2/CuO heterostructure on fluorine-doped tin oxide (FTO) as an efficient light-harvesting photoanode to generate H_2 through the water-splitting process. Reisner and co-workers [137] have studied the photoelectrochemical water oxidation with a catalyst called Photosystem (PSII) integrated in a mesoporous indium-tin oxide (mesoITO) electrode is shown in Fig. 18.14. In this study, a hybrid photoanode consisting of the combination of a biological catalyst and a 3D, biocompatible, solid-state material for water oxidation is presented. The catalyst, PSII isolated from the thermophilic cyanobacterium Thermosynechococcus elongatus was integrated in a mesoITO electrode. The transmembrane protein complex PSII contains highly sophisticated machinery for light absorption, charge separation, and water oxidation catalysis. It provides the best means available for the oxidation of water in terms of catalytic rate and, therefore, provides a reference point for synthetic systems. Also, mesoITO proved to be an excellent and emerging electrode material as it allows for

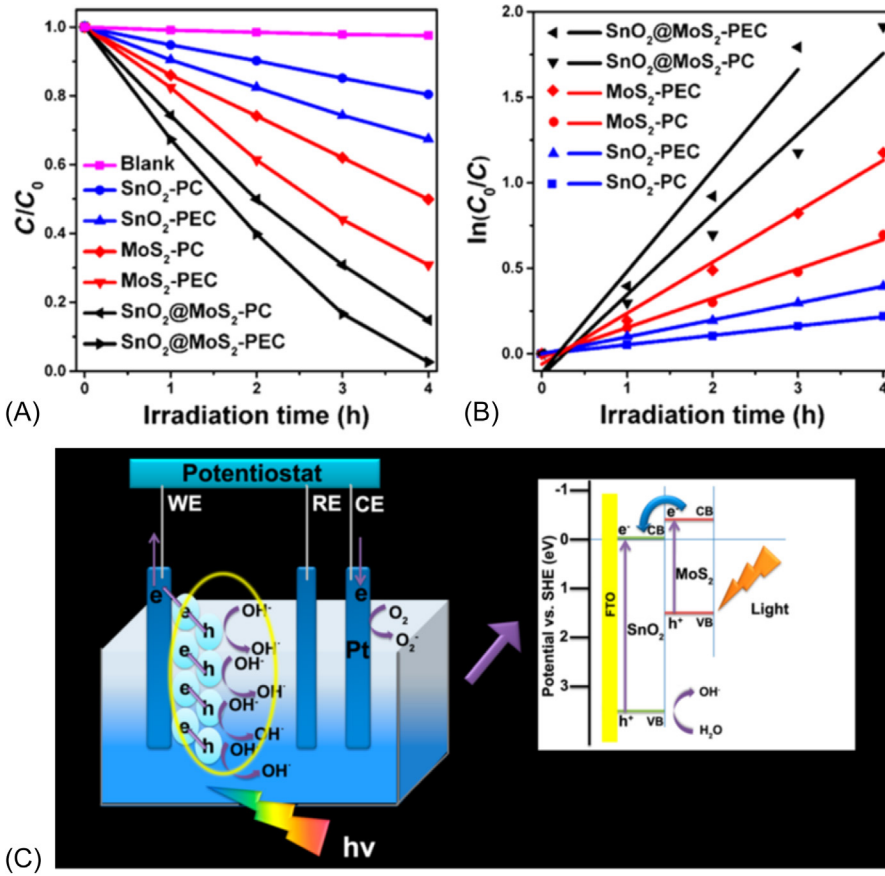

Fig. 18.13 (A) Photocatalytic (PC) and photoelectrocatalytic (PEC) degradation; (B) linear fitting of pseudo-first-order kinetics of rhodamine B degradation; and (C) schematic illustration of the energy band structure and the PEC degradation process of the SnO_2@MoS_2 film under visible light.
Reprinted with permission from Zhang X, Yang Y, Ding S, Que W, Zheng Z, Du Y. Inorg Chem, 2017;56:3386–3393. Copyright (2017) ACS.

high enzyme catalyst loading, high electrical conductivity, and an optical transparency as required for photoelectrochemical experiments. Mullins and his group [138] have reported the growth of well-defined antimony-doped tin oxide (ATO) nanorods as a conductive scaffold to improve hematite's photoelectrochemical water oxidation performance. They found that the hematite grown on ATO exhibits greater performance for photoelectrochemical water oxidation compared to hematite grown on flat FTO. The optimized photocurrent density of hematite on ATO is 0.67 mA/cm^2 (0.6 V vs Ag/AgCl), which is much larger than the photocurrent density of hematite on flat FTO (0.03 mA/cm^2). In addition to this, SnO_2 was studied with a variety of combination such as SnO_2/$BiVO_4$ core-shell heterostructures [139], SnO_2@$BiVO_4$/Co-Pi [140], SnO_2/TiO_2 nanotubes [141], and so on for photoelectocatalysis applications.

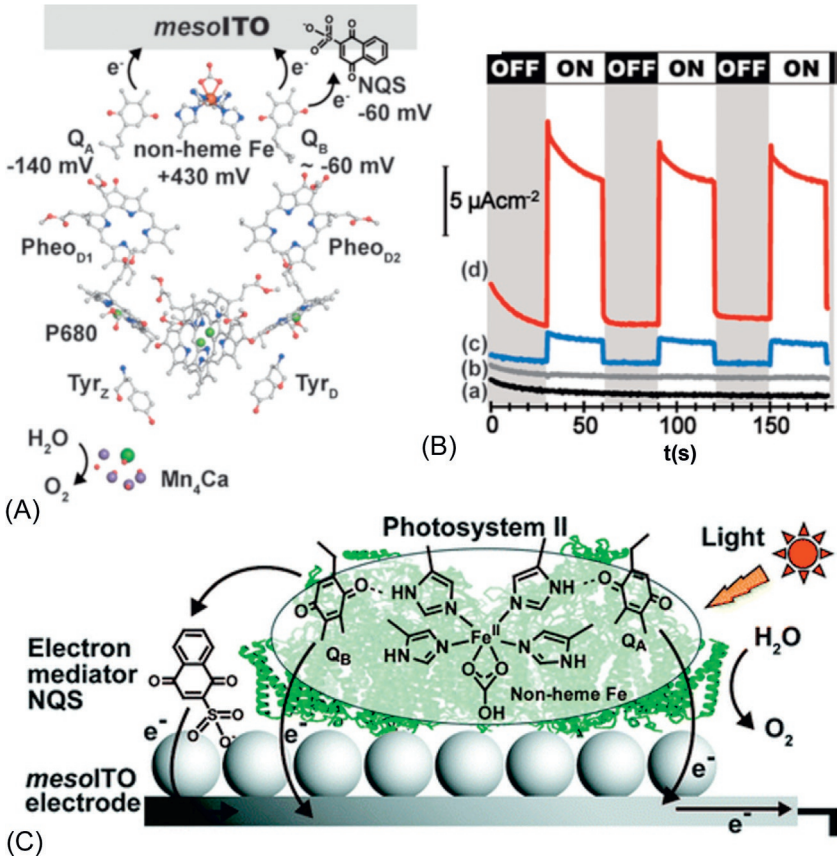

Fig. 18.14 (A) Schematic representation of the arrangement of cofactors involved in an electron transfer chain in PSII and the redox potentials of Q_A, Q_B, the nonheme iron, and NQS; (B) representative photocurrent response of unmodified *meso*ITO (a), [Mn_4Ca]-cluster depleted-PSII-*meso*ITO (b), PSII-*meso*ITO (c) and PSII-*meso*ITO with 1 mM NQS (d); and (C) schematic representation of the reaction mechanism involved in photosystem II (PSII) integrated in a mesoporous indium-tin oxide electrode.
Reprinted with permission from Kato M, Cardona T, Rutherford AW, Reisner E. J Am Chem Soc 2012;134:8332–8335. Copyright (2012) ACS.

18.7 Conclusive remarks

Among different metal oxides, tin oxide has attracted a lot of attention in the recent years for different applications due to its unique electronic and chemical properties. SnO_2 with lower percentage of ionic character and higher oxidation state of Sn (4+) was found to contain higher acidity which can catalyze some important organic reactions. Its catalytic properties can be improved by creating mesoporosity and higher surface area by template-assisted synthesis and calcination procedure. Mesoporous tin oxide efficiently catalyzed reactions like Prins reaction to produce nopol and glycerol

condensation with acetone to give solketal. The product yield obtained for solketal was higher compared to mesoporous aluminosilicates and conventional zeolite catalysts. Tin oxide was also effectively combined with other oxides to make mixed and composite oxides which further enhanced its catalytic properties. Zinc-tin composite oxide synthesized by coprecipitation method calcined at 600 °C was a better catalyst for carbonylation of glycerol with urea to produce glycerol carbonate. Higher concentration of Zn_2SnO_4 phase in Zn−Sn composite oxide was found to improve both acidity and basicity and hence better catalytic activity was achieved. Tin-tungsten mixed oxide was a well-studied catalyst which was utilized in variety of organic transformations like cyclization of citronellal, Diels-Alder reaction, cyanoethylation, hydration of aldoximes to nitriles, hydration of alkynes, carbonylation of glycerol, and isomerization of glucose and fructose. The catalytic activity of tin-tungsten mixed oxide calcined at 800°C was much higher than that of acid-type zeolites such as H-MOR and H−Y for cyclization of citronellal reaction. SnO_2 is also used as a catalyst support by impregnating anion or cation (M/SnO_2 (M = Ca, Si, WO_3, MoO_3, Pd, and more), HPA/SnO_2, SO_4^{2-}/SnO_2) on the catalyst surface followed by calcination to generate active sites which is used for various organic reactions. SnO_2 as a support improved the heterogeneity and thermal stability of heteropoly acids, and improved the catalytic activity in alkylation reactions. Thus, the researchers explored the utilization of SnO_2 in catalysis by tuning its physicochemical properties, mainly porosity, surface area, acidity, and basicity either in its pure form or by mixing with other metal oxides, acids, bases, or varying calcination temperature. Such SnO_2 materials with tuned properties are found to be excellent catalysts for variety of organic transformations. Tin oxide found to be very effective in photocatalytic applications namely degradation of dyes and hydrogen generation reactions. It has also received much attention as a photoanode for photoelectrocatalysis because of its favorable energy-level position, high photoactivity, excellent resistance for photocorrosion, chemical stability, electron transport properties, and low cost. Its properties are further improved by combining with other materials like MoS_2 to make nanohybrids for the degradation of dyes and water splitting reactions.

It is evident that the ease of synthesis and the exceptional tuneable properties in tin oxide proved it as a versatile material for various noteworthy applications. A few changes in the synthesis method can provide an extraordinary feature in tin oxide/tin oxide-based materials. The properties such as acidity, basicity, and redox can be tuned through the incorporation of other metal ions in the structure to form a mixed metal oxide. The influence of other metal in tin oxide environment can alter its physicochemical properties, thereby enhancing its catalytic behavior due to the synergistic effect. It can also act as a potential catalyst or support due to its redox properties. A better control over the synthesis to achieve a desired combination of Brönsted and Lewis acidity without losing total acidity is yet to be accomplished. Also, the structure-activity correlation for SnO_2-based catalysts is less understood in many organic transformations. There is still a scope to further improve properties of SnO_2 by tuning and appropriate modifications using innovative methods and apply in variety of commercially important reactions like alkylation, acylation, esterification, etherification, and oxidation which are less explored so far with this material.

References

[1] Schlögl R. Angew Chem Int Ed 2015;54:3465–520.
[2] Somorjai GA, McCrea K. Appl Catal Gen 2001;222:3–18.
[3] Zaera F. Chem Soc Rev 2013;42:2746–62.
[4] Thomas JM, Ducati C, Leary R, Midgley PA. ChemCatChem 2013;5:2560–79.
[5] Armor JN. Catal Today 2011;163:3–9.
[6] Ma Z, Zaera F. Heterogeneous catalysis by metals. In: Encyclopedia of inorganic and bioinorganic chemistry. John Wiley & Sons, Ltd; 2014.
[7] Bravo-Suárez JJ, Chaudhari RV, Subramaniam B. ACS Symp Ser 2013;1132:3–68.
[8] https://www.transparencymarketresearch.com/pressrelease/global-refinery-catalyst-market.htm.
[9] Anastas P, Eghbali N. Chem Soc Rev 2010;39:301–12.
[10] Mitchell S, Michels N-L, Pérez-Ramírez J. Chem Soc Rev 2013;42:6094–112.
[11] Jacobs PW, Somorjai GA. J Mol Catal A Chem 1998;131:5–18.
[12] Wachs IE. Catal Today 2005;100:79–94.
[13] Cychosz KA, Guillet-Nicolas R, García-Martínez J, Thommes M. Chem Soc Rev 2017;46:389–414.
[14] Helveg S. J Catal 2015;328:102–10.
[15] Thomas JM, Thomas WJ. Principles and practice of heterogeneous catalysis. John Wiley & Sons; 2014.
[16] Pal N, Bhaumik A. RSC Adv 2015;5:24363–91.
[17] Parlett CM, Wilson K, Lee AF. Chem Soc Rev 2013;42:3876–93.
[18] Batzill M, Diebold U. Prog Surf Sci 2005;79:47–154.
[19] Chen Z, Pan D, Li Z, Jiao Z, Wu M, Shek C-H, Wu CL, Lai JK. Chem Rev 2014;114:7442–86.
[20] Varala R, Narayana V, Kulakarni SR, Khan M, Alwarthan A, Adil SF. Arab J Chem 2016;9:550–73.
[21] Greenwood NN, Earnshaw A. Chemistry of the elements. 1984.
[22] Bae J-Y, Park J, Kim HY, Kim H-S, Park J-S. ACS Appl Mater Interfaces 2015;7:12074–9.
[23] Toupance T, El Hamzaoui H, Jousseaume B, Riague H, Saadeddin I, Campet G, Brötz J. Chem Mater 2006;18:6364–72.
[24] Ihokura K, Watson J. The stannic oxide gas sensor principles and applications. CRC press; 2017.
[25] Khodadadi A, Mohajerzadeh S, Mortazavi Y, Miri A. Sensors Actuators B Chem 2001;80:267–71.
[26] Zhang Y, Liu Y, Liu M. Chem Mater 2006;18:4643–6.
[27] Toupance T, Babot O, Jousseaume B, Vilaça G. Chem Mater 2003;15:4691–7.
[28] Harrison PG, Bailey C, Azelee W. J Catal 1999;186:147–59.
[29] Mallesham B, Sudarsanam P, Raju G, Reddy BM. Green Chem 2013;15:478–89.
[30] Raveendra G, Surendar M, Prasad PS. N J Chem 2017;41:8520–9.
[31] Marakatti VS, Manjunathan P, Halgeri AB, Shanbhag GV. Cat Sci Technol 2016;6:2268–79.
[32] Manjunathan P, Marakatti VS, Chandra P, Kulal AB, Umbarkar SB, Ravishankar R, Shanbhag GV. Catal Today 2018;309:61–76.
[33] Satam JR, Gawande MB, Deshpande SS, Jayaram RV. Synth Commun 2007;37:3011–20.
[34] Dabbawala AA, Mishra DK, Hwang J-S. Catal Commun 2013;42:1–5.
[35] Ogasawara Y, Uchida S, Yamaguchi K, Mizuno N. Chem A Eur J 2009;15:4343–9.

[36] Khder A, Ahmed A. Appl Catal Gen 2009;354:153–60.
[37] Misono M. Stud Surf Sci Catal 2013;25–65.
[38] San Kong P, Aroua MK, Daud WMAW, Lee HV, Cognet P, Pérès Y. RSC Adv 2016;6:68885–905.
[39] Corma A. Chem Rev 1997;97:2373–420.
[40] Ciesla U, Schüth F. Microporous Mesoporous Mater 1999;27:131–49.
[41] Kresge C, Leonowicz M, Roth WJ, Vartuli J, Beck J. Nature 1992;359:710.
[42] Beck JS, Vartuli J, Roth WJ, Leonowicz M, Kresge C, Schmitt K, Chu C, Olson DH, Sheppard E, McCullen S. J Am Chem Soc 1992;114:10834–43.
[43] Celdeira PA, Goncalves M, Figueiredo FC, Dal Bosco SM, Mandelli D, Carvalho WA. Appl Catal Gen 2014;478:98–106.
[44] Moritz M, Geszke-Moritz M. Mater Sci Eng C 2015;49:114–51.
[45] Lee C-H, Lin T-S, Mou C-Y. Nano Today 2009;4:165–79.
[46] Huo Q, Margolese DI, Ciesla U, Feng P, Gier TE, Sieger P, Leon R, Petroff PM, Schüth F, Stucky GD. Nature 1994;368:317.
[47] Wang Y, Ma C, Sun X, Li H. J Colloid Interface Sci 2005;286:627–31.
[48] Bagshaw SA, Pinnavaia TJ. Angew Chem Int Ed 1996;35:1102–5.
[49] Antonelli DM, Ying JY. Angew Chem Int Ed 1995;34:2014–7.
[50] Antonelli DM, Ying JY. Angew Chem Int Ed 1996;35:426–30.
[51] Pacheco G, Zhao E, Garcia A, Sklyarov A, Fripiat J. Chem Commun 1997;491–2.
[52] Gu D, Schüth F. Chem Soc Rev 2014;43:313–44.
[53] Mohanty P, Ortalan V, Browning ND, Arslan I, Fei Y, Landskron K. Angew Chem Int Ed 2010;49:4301–5.
[54] Wang Y, Ma C, Sun X, Li H. Microporous Mesoporous Mater 2001;49:171–8.
[55] Wang Y-D, Ma C-L, Sun X-D. Inorg Chem Commun 2001;4:223–6.
[56] Antonelli DM, Nakahira A, Ying JY. Inorg Chem 1996;35:3126–36.
[57] Crepaldi EL, Soler-Illia GJdA, Grosso D, Cagnol F, Ribot F, Sanchez C. J Am Chem Soc 2003;125:9770–86.
[58] Fan J, Boettcher SW, Stucky GD. Chem Mater 2006;18:6391–6.
[59] Ulagappan N, Rao C. Chem Commun 1996;1685–6.
[60] Pal N, Bhaumik A. Adv Colloid Interface Sci 2013;189:21–41.
[61] Roggenbuck J, Schäfer H, Tsoncheva T, Minchev C, Hanss J, Tiemann M. Microporous Mesoporous Mater 2007;101:335–41.
[62] Dupont L, Laruelle S, Grugeon S, Dickinson C, Zhou W, Tarascon J-M. J Power Sources 2008;175:502–9.
[63] Jiao F, Harrison A, Hill AH, Bruce PG. Adv Mater 2007;19:4063–6.
[64] Kumar S, Malik M, Purohit R. Mater Today Proc 2017;4:350–7.
[65] Gawande MB, Pandey RK, Jayaram RV. Cat Sci Technol 2012;2:1113–25.
[66] Marakatti VS, Shanbhag GV, Halgeri AB. RSC Adv 2013;3:10795–800.
[67] Chu X, Zhou D, Li D, Xia K, Gan N, Lu X, Nie R, Xia Q. Microporous Mesoporous Mater 2016;230:166–76.
[68] Jadhav SV, Jinka KM, Bajaj HC. Catal Today 2012;198:98–105.
[69] Opanasenko M, Dhakshinamoorthy A, Hwang YK, Chang JS, Garcia H, Čejka J. ChemSusChem 2013;6:865–71.
[70] Melero JA, Vicente G, Morales G, Paniagua M, Bustamante J. Fuel 2010;89:2011–8.
[71] Climent MJ, Corma A, Iborra S. Green Chem 2014;16:516–47.
[72] Manjunathan P, Maradur SP, Halgeri A, Shanbhag GV. J Mol Catal A Chem 2015;396:47–54.

[73] Churipard SR, Manjunathan P, Chandra P, Shanbhag GV, Ravishankar R, Rao PV, Ganesh GS, Halgeri A, Maradur SP. N J Chem 2017;41:5745–51.
[74] Sandesh S, Halgeri A, Shanbhag GV. J Mol Catal A Chem 2015;401:73–80.
[75] Cousin P, Ross R. Mater Sci Eng A 1990;130:119–25.
[76] Hattori H. Appl Catal Gen 2001;222:247–59.
[77] Parameswaram G, Srinivas M, Babu BH, Prasad PS, Lingaiah N. Cat Sci Technol 2013;3:3242–9.
[78] Hattori H. Chem Rev 1995;95:537–58.
[79] Hattori H, Ono Y. Solid acid catalysis: from fundamentals to applications. Pan stanford; 2015, ISBN: 9789814463287.
[80] Manjunathan P, Ravishankar R, Shanbhag GV. ChemCatChem 2016;8:631–9.
[81] Yamaguchi K, Sakurada T, Ogasawara Y, Mizuno N. Chem Lett 2011;40:542–3.
[82] Xie W, Wang T. Fuel Process Technol 2013;109:150–5.
[83] Jagadeeswaraiah K, Kumar CR, Prasad PS, Loridant S, Lingaiah N. Appl Catal Gen 2014;469:165–72.
[84] Jin X, Oishi T, Yamaguchi K, Mizuno N. Chem A Eur J 2011;17:1261–7.
[85] Peng H, Liu Y, Li Y, Zhang X, Tang X, Xu X, Fang X, Liu W, Zhang N, Wang X. ChemCatChem 2016;8:2329–34.
[86] Wang C-T, Lai D-L, Chen M-T. Appl Surf Sci 2010;257:127–31.
[87] Sandesh S, Kristachar PKR, Manjunathan P, Halgeri A, Shanbhag GV. Appl Catal Gen 2016;523:1–11.
[88] Sandesh S, Shanbhag GV, Halgeri A. RSC Adv 2014;4:974–7.
[89] Li H, Gao D, Gao P, Wang F, Zhao N, Xiao F, Wei W, Sun Y. Cat Sci Technol 2013;3:2801–9.
[90] Hino M, Takasaki S, Furuta S, Matsuhashi H, Arata K. Appl Catal Gen 2007;321:147–54.
[91] Corma A, Renz M. Chem Commun 2004;550–1.
[92] Imachi S, Owada K, Onaka M. J Mol Catal A Chem 2007;272:174–81.
[93] Chuah G, Liu S, Jaenicke S, Harrison L. J Catal 2001;200:352–9.
[94] Jacob RG, Perin G, Loi LN, Pinno CS, Lenardão EJ. Tetrahedron Lett 2003;44:3605–8.
[95] Corma A. Chem Rev 1995;95:559–614.
[96] Zhang Z, Zhu Q, Ding J, Liu X, Dai W-L. Appl Catal Gen 2014;482:171–8.
[97] Mallesham B, Sudarsanam P, Reddy BM. Cat Sci Technol 2014;4:803–13.
[98] Mallesham B, Sudarsanam P, Reddy BM. Ind Eng Chem Res 2014;53:18775–85.
[99] Ahmed AI, El-Hakam S, Elghany MA, El-Yazeed WA. Appl Catal Gen 2011;407:40–8.
[100] Sekizawa K, Widjaja H, Maeda S, Ozawa Y, Eguchi K. Appl Catal Gen 2000;200:211–7.
[101] Xie W, Zhao L. Energ Conver Manage 2013;76:55–62.
[102] Kouzu M, Yamanaka S-y, Hidaka J-s, Tsunomori M. Appl Catal Gen 2009;355:94–9.
[103] Granados ML, Alonso DM, Sádaba I, Mariscal R, Ocón P. Appl Catal Environ 2009;89:265–72.
[104] Samart C, Chaiya C, Reubroycharoen P. Energ Conver Manage 2010;51:1428–31.
[105] Kozhevnikov IV. Chem Rev 1998;98:171–98.
[106] Okuhara T. Catal Today 2002;73:167–76.
[107] Kozhevnikov I. J Mol Catal A Chem 2009;305:104–11.
[108] Izumi Y, Ono M, Kitagawa M, Yoshida M, Urabe K. Microporous Mater 1995;5:255–62.
[109] Alsalme A, Kozhevnikova EF, Kozhevnikov IV. Appl Catal Gen 2008;349:170–6.
[110] Shimizu K-i, Niimi K, Satsuma A. Appl Catal Gen 2008;349:1–5.
[111] Shanbhag GV, Palraj K, Halligudi S. Open Org Chem J 2008;2:52–7.
[112] Sandesh S, Manjunathan P, Halgeri AB, Shanbhag GV. RSC Adv 2015;5:104354–62.
[113] Kumbar SM, Shanbhag G, Lefebvre F, Halligudi S. J Mol Catal A Chem 2006;256:324–34.

[114] Devassy BM, Shanbhag G, Lefebvre F, Halligudi S. J Mol Catal A Chem 2004;210:125–30.
[115] Abd El Rahman SK. Appl Catal Gen 2008;343:109–16.
[116] Kumar CR, Prasad PS, Lingaiah N. Appl Catal Gen 2010;384:101–6.
[117] Srilatha K, Kumar CR, Devi BP, Prasad R, Prasad PS, Lingaiah N. Catal Sci Technol 2011;1:662–8.
[118] Abd El Rahman SK, Hassan HM, El-Shall MS. Appl Catal Gen 2012;411:77–86.
[119] Tsukuda E, Sato S, Takahashi R, Sodesawa T. Catal Commun 2007;8:1349–53.
[120] Srinivas M, Raveendra G, Parameswaram G, Prasad PS, Lingaiah N. J Mol Catal A Chem 2016;413:7–14.
[121] Bhattacharjee A, Ahmaruzzaman M. Mater Lett 2015;139:418–21.
[122] Bhattacharjee A, Ahmaruzzaman M. Mater Lett 2015;145:74–8.
[123] Bhattacharjee A, Ahmaruzzaman M. J Colloid Interface Sci 2015;448:130–9.
[124] Mohanta D, Ahmaruzzaman M. RSC Adv 2016;6:110996–1015.
[125] Pan R, Pan S, Zhou J, Wu Y. Appl Surf Sci 2009;255:3642–7.
[126] Sinha AK, Pradhan M, Sarkar S, Pal T. Environ Sci Technol 2013;47:2339–45.
[127] Velaga B, Shanbogh PP, Swain D, Narayana C, Sundaram NG. Photochem Photobiol 2018;94:633–40.
[128] Hosogi Y, Shimodaira Y, Kato H, Kobayashi H, Kudo A. Chem Mater 2008;20:1299–307.
[129] Ghosh M, Pralong V, Wattiaux A, Sleight A, Subramanian M. Chem Asian J 2009;4:881–5.
[130] Boppana VBR, Lobo RF. J Catal 2011;281:156–68.
[131] Long J, Xue W, Xie X, Gu Q, Zhou Y, Chi Y, Chen W, Ding Z, Wang X. Catal Commun 2011;16:215–9.
[132] Manikandan M, Tanabe T, Li P, Ueda S, Ramesh GV, Kodiyath R, Wang J, Hara T, Dakshanamoorthy A, Ishihara S. ACS Appl Mater Interfaces 2014;6:3790–3.
[133] Zhang X, Yang Y, Ding S, Que W, Zheng Z, Du Y. Inorg Chem 2017;56:3386–93.
[134] Yao T, An X, Han H, Chen JQ, Li C. Adv Energy Mater 2018;8:1800210.
[135] Chen JS, Lou XW. Small 2013;9:1877–93.
[136] Yin Z, Wang Z, Du Y, Qi X, Huang Y, Xue C, Zhang H. Adv Mater 2012;24:5374–8.
[137] Kato M, Cardona T, Rutherford AW, Reisner E. J Am Chem Soc 2012;134:8332–5.
[138] Sun Y, Chemelewski WD, Berglund SP, Li C, He H, Shi G, Mullins CB. ACS Appl Mater Interfaces 2014;6:5494–9.
[139] Bera S, Lee SA, Kim C-M, Khan H, Jang HW, Kwon S-H. Chem Mater 2018;30:8501–9.
[140] Liu J, Li J, Shao M, Wei M. J Mater Chem A 2019.
[141] Chai S, Zhao G, Li P, Lei Y, Zhang Y-n, Li D. J Phys Chem C 2011;115:18261–9.